The FEBS Journal

FEBS PRESS science publishing by scientists

Antitumour drugs targeting tau R3 VQIVYK and Cys322 prevent seeding of endogenous tau aggregates by exogenous seeds

Narendran Annadurai[1], Lukáš Malina[2], Mario Salmona[3], Luisa Diomede[3], Antonio Bastone[3], Alfredo Cagnotto[3], Margherita Romeo[3], Martin Šrejber[4], Karel Berka[5], Michal Otyepka[4,6], Marián Hajdúch[1] and Viswanath Das[1]

1 Institute of Molecular and Translational Medicine, Faculty of Medicine and Dentistry, Palacký University Olomouc, Olomouc, Czech Republic
2 Department of Medical Biophysics, Faculty of Medicine and Dentistry, Palacký University in Olomouc, Olomouc, Czech Republic
3 Department of Molecular Biochemistry and Pharmacology, Istituto di Ricerche Farmacologiche Mario Negri IRCCS, Milan, Italy
4 Czech Advanced Technology and Research Institute (CATRIN), Regional Centre of Advanced Technologies and Materials (RCPTM), Palacký University Olomouc, Olomouc, Czech Republic
5 Department of Physical Chemistry, Faculty of Science, Palacký University Olomouc, Olomouc, Czech Republic
6 IT4Innovations, VSB – Technical University of Ostrava, Ostrava, Czech Republic

Keywords
Alzheimer's disease; antitumour agents; prion-like; tau aggregation; tau seeding

Correspondence
V. Das, Faculty of Medicine and Dentistry, Institute of Molecular and Translational Medicine, Palacký University Olomouc Hněvotínská 5, 77900 Olomouc, Czech Republic
Tel: +420 585 632 111
E-mail: viswanath.das@upol.cz

(Received 28 June 2021, revised 1 October 2021, accepted 5 November 2021)

doi:10.1111/febs.16270

Emerging experimental evidence suggests tau pathology spreads between neuroanatomically connected brain regions in a prion-like manner in Alzheimer's disease (AD). Tau seeding, the ability of prion-like tau to recruit and misfold naïve tau to generate new seeds, is detected early in human AD brains before the development of major tau pathology. Many antitumour drugs have been reported to confer protection against neurodegeneration, supporting the repurposing of approved and experimental or investigational oncology drugs for AD therapy. In this study, we evaluated whether antitumour drugs that abrogate the generation of seed-competent aggregates of tau Repeat 3 (R3) domain peptides can prevent tau seeding and toxicity in Tau-RD P301S FRET Biosensor cells and *Caenorhabditis elegans*. We demonstrate that drugs that interact with the N-terminal VQIVYK or the C-terminal region housing the Cys322 prevent R3 dimerisation, abolishing the generation of prion-like R3 seeds. Preformed R3 seeds (fibrils) capped with, or R3 seeds formed in the presence of VQIVYK- or Cys322-targeting drugs have a reduced potency to cause aggregation of naïve tau in biosensor cells and protect worms from aggregate toxicity. These findings indicate that VQIVYK- or Cys322-targeting drugs may act as prophylactic agents against tau seeding.

Introduction

Intracytoplasmic neurofibrillary tau tangles and extracellular plaques of amyloid-β (Aβ) are two histopathological characteristics of Alzheimer's disease (AD). But why does the disease progress rapidly in some typical AD patients while the disease develops gradually over decades in others? Answers to this question may partly come from the pathological tau species that develop early in AD brains and spread between connected neurons in a prion-like manner [1]. Circumstantial evidence shows that pathological 'tau seeds' spread across

Abbreviations
AD, Alzheimer's disease; AFM, atomic force microscopy; Aβ, amyloid-β; DMF, dimethylformamide; MD, molecular dynamics; NGM, nematode growth medium; R3, repeat 3; R3Ags, R3 aggregates; ThT, thioflavin T.

the brain through synaptically connected neurons, potentially contributing to AD pathogenesis [2–8]. Clinically, the presence of tau precedes significant grey matter atrophy in AD brains, suggesting tau as a critical inducer of neurodegeneration [9]. Evidence from tau PET imaging data also reveals that tau spreading is not limited to just AD but also occur in normal ageing brains and that the presence of Aβ accelerates this process [3].

The nucleation-dependent tau aggregation displays a typical sigmoidal shape curve similar to Aβ aggregation [10]. The nucleation phase involves the assembly of critical nuclei, to which monomeric units are added, driving the assembly of oligomers. However, targeting oligomers prevent oligomer-mediated neurotoxicity [11]. For example, bexarotene-mediated blocking of primary nucleation of Aβ inhibits oligomer generation and associated toxicity [12]. In addition, there are indications that nucleation events in tau aggregation may become active in AD at early stages [10] and possibly tau seeding [2,5]. Thus, interfering at the nucleation phase may block pathological seed generation, such as blocking toxic Aβ oligomers.

Two amyloid motifs, VQIINK in Repeat 2 and VQIVYK in Repeat 3 (R3), present in the repeat region, are critical for tau nucleation [10]. Peptide-like inhibitors targeting a particular interface of VQIVYK in AD patient-derived fibrils block seeding [13]. An essential step in the nucleation phase that precedes higher-molecular-weight or low-molecular-weight oligomer formation is the dimerisation of tau through disulfide bonding of cysteine residues [14]. Oxidation of these cysteines results in small tau conformers ranging from dimers to oligomers actively participating in tau spreading [15]. Catechol that caps cysteine residues impedes tau dimerisation and oligomer formation, preventing neuronal death and brain dysfunctions in P301L tau transgenic mice [16].

Several retrospective studies indicate that cancer survivors have a reduced risk of dementia and AD development than individuals without cancer [17–20]. Whether this inverse correlation is due to a common biological mechanism shared between cancer and AD patients or pharmacological interventions in cancer patients remains debated [20–24]. The underlying mechanisms for the reduced risk of AD in cancer survivors are primarily unknown. Different drugs may target different pathways to lower AD development [25], but evidence suggests that chemotherapy reduce AD risk in cancer survivors [24–27]. Given that chemotherapy preceded AD diagnosis in cancer survivors in the retrospective studies [17–20], we speculated that chemotherapy drugs abrogate the formation of tau seeds to prevent tau spreading and AD development. We tested a panel of twenty approved and four experimental or investigational antitumour drugs to identify inhibitors of tau nucleation, thereby abrogating the generation of prion-like seeds and seeding. The effects of selected drugs on the seeding of endogenous tau by exogenous aggregates of tau Repeat 3 (R3) domain peptides were studied using Tau-RD P301S FRET Biosensor cells [26]. The *in vivo* toxicity of peptide aggregates, with or without prior drug treatment, was examined in *Caenorhabditis elegans*, which recognises amyloidogenic proteins as toxic by inhibiting their feeding behaviour.

Results

R3 aggregation and effects of antitumour drugs on their fibrillisation

We first monitored the assembly of R3 peptides into fibrils under four aggregation conditions by thioflavin T (ThT) binding assay to determine an optimal condition for drug screening (Fig. 1A). R3 showed distinct behaviours under reducing (+heparin/+DTT) aggregation conditions. The presence of dithiothreitol (DTT) affected the assembly of R3 peptides even in the absence of heparin. Our data and evidence from a previous study show a differential effect of heparin and DTT on fibrillisation kinetics of tau isoforms containing either Cys291 or Cys322 residue [14]. Therefore, we decided to test drug effects on peptide aggregation in the absence of DTT. Moreover, DTT was also excluded from drug screening to avoid possible false-positive results due to the oxidation of Cys322 by hydrogen peroxide generated by redox cycling compounds in the presence of reducing agents [27]. Atomic force microscopy (AFM) analysis showed R3 assembled into amyloidogenic fibrils 48 h after aggregation (Fig. 1B).

Next, we explored the effect of 20 approved and four experimental or investigational antitumour drugs on *in vitro* aggregation of R3 (Table 1). These drugs were selected randomly on their availability in our laboratory. The fibrillisation of peptides was first monitored in the presence of drugs at a single concentration (1-μM) by ThT assay (Fig 1C). A comparison of the ThT fluorescence reading showed that paclitaxel, docetaxel, cisplatin, oxaliplatin, doxorubicin, daunorubicin, resveratrol and quercetin resulted in a significant decrease (> 50%) in ThT fluorescence at the 1 μM tested concentration compared to control reaction without drugs (Table 2). For subsequent *in vitro* studies, we selected paclitaxel, cisplatin, doxorubicin, resveratrol and quercetin and tested the effect of the five drugs on peptide fibrillisation at two additional doses of 0.1 and 10 μM. Whereas the effect of paclitaxel did not alter with

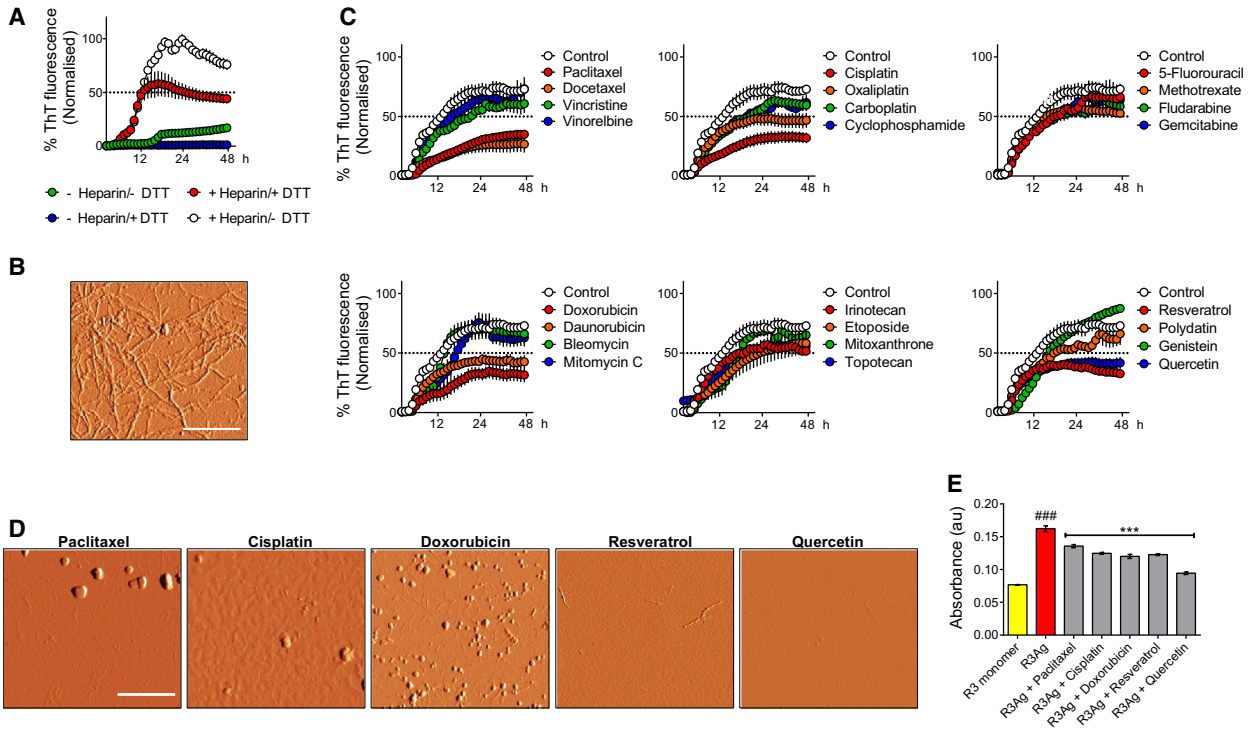

Fig. 1. Drug effect on R3 aggregation. (A) Graphs showing the rate of R3 aggregation under different conditions. (B) AFM image of R3 fibrils 48 h after incubation under nonreducing conditions. Scale bar: 2 μm. (C) Effect of antitumour drugs from groups 1 to 6 at a single concentration of 1-μM on R3 aggregation. (D) AFM images showing the morphology of R3Ags after 48 h of aggregation in the presence of indicated drugs at a concentration of 10 μM. Scale bar: 2 μm. (E) Congo red absorbance of R3 monomer and R3Ags after 48 h of aggregation in the absence or presence of indicated drugs at 10 μM concentration. Congo red was added immediately before reading the absorbance. Data in A, C and E are mean ± SEM, $n = 3$–4 independent experiments. $^{***}P < 0.001$ vs R3Ag; and $^{###}P < 0.001$ vs R3 monomer, one-way ANOVA, Bonferroni's *post hoc* test.

Table 1. List of antitumour drugs classified into six groups based on their primary mechanism of action.

Approved					Preclinical/clinical
Group 1. Antitubulin agents	Group 2. Alkylating agents	Group 3. Antimetabolites	Group 4. Antibiotics	Group 5. Topoisomerase	Group 6. Antioxidants
Paclitaxel	Cisplatin	5-fluorouracil	Doxorubicin	Irinotecan	Resveratrol
Docetaxel	Oxaliplatin	Methotrexate	Daunorubicin	Etoposide	Polydatin
Vincristine	Carboplatin	Fludarabine	Bleomycin	Mitoxantrone	Lycopene
Vinorelbine	Cyclophosphamide	Gemcitabine	Mitomycin C	Topotecan	Quercetin

the change in its concentration, cisplatin, doxorubicin, resveratrol and quercetin were more effective at 10 μM in inhibiting R3 fibrillisation (Fig. S1A). DMSO as a drug solvent did not affect R3 fibrillisation at the tested drug concentrations (Fig. S1B), and doxorubicin or daunorubicin-intrinsic fluorescence did not interfere with ThT fluorescence in our assay condition (Fig. S1C).

AFM analysis of R3 peptides 48 h after aggregation in the presence of 10-μM paclitaxel, cisplatin, resveratrol and quercetin showed a complete absence of fibril formation (Fig. 1D). In contrast, the formation of small granular to short fibril-like aggregates was observed in the presence of doxorubicin (Fig. 1D). Overall, these results suggest that paclitaxel, cisplatin, doxorubicin, resveratrol and quercetin limited the conversion of peptides from a soluble form to insoluble fibrillary aggregates.

Although ThT assay is frequently used to detect amyloid fibrils, resveratrol and quercetin have been

Table 2. Comparison of ThT fluorescence reading from Fig. 1C. The final (48th hour) normalised ThT fluorescence values following aggregation of R3 peptides in the presence of indicated drugs at a concentration of 1 μM. Mean ± SEM, drugs vs control, one-way ANOVA, Dunnett's *post hoc* test. Not significant, ns.

%ThT fluorescence (normalised)		
	Mean ± SEM	*P*-values
Control	74 ± 3	
Paclitaxel	35 ± 2	0.002
Docetaxel	27 ± 7	< 0.001
Vincristine	60 ± 7	0.386
Vinorelbine	73 ± 10	> 0.999
Cisplatin	32 ± 5	< 0.001
Oxaliplatin	46 ± 6	0.002
Carboplatin	69 ± 10	0.149
Cyclophosphamide	84 ± 15	0.422
5-fluorouracil	56 ± 6	0.247
Methotrexate	51 ± 2	0.089
Fludarabine	60 ± 9	0.432
Gemcitabine	63 ± 11	0.641
Doxorubicin	31 ± 6	< 0.001
Daunorubicin	42 ± 6	0.002
Bleomycin	70 ± 7	0.976
Mitomycin C	61 ± 8	0.353
Irinotecan	52 ± 4	0.019
Etoposide	58 ± 10	0.150
Mitoxantrone	60 ± 5	0.232
Topotecan	56 ± 3	0.058
Resveratrol	32 ± 2	< 0.001
Polydatin	59 ± 7	0.054
Genistein	89 ± 2	0.071
Quercetin	41 ± 5	< 0.001

reported to compete with ThT for amyloid binding [28]. Therefore, we also confirmed the antifibrillisation effects of drugs by an end-point fluorescence microscopy analysis. R3 peptide was assembled in the absence or presence of drugs under a proaggregation condition but without ThT. After 48 h, the content of the plate well was embedded in agarose, followed by imaging (Fig. S1D). We also performed an end-point Congo red binding assay to validate the antifibrillisation activity of drugs, particularly resveratrol and quercetin. A decreased Congo red absorbance in samples of R3 aggregates (R3Ags) assembled in the presence of drugs substantiated the antifibrillisation activity of drugs (Fig 1E). Overall, since ThT was added at the end of the aggregation assay for fluorescence microscopy analysis and Congo red binding assay, our findings confirm that drugs inhibit the formation of β-sheet-rich aggregates, and there is no interference of ThT to binding to R3 in the presence of drugs.

Inhibition of polymerisation of preformed R3 fibrils

Neurofibrillary tangles (NFTs) are formed in the advanced stages of the disease, whereas soluble oligomers generated at early stages are more toxic tau species responsible for neuronal death [29]. Therefore, we next determined whether drugs that inhibited fibrillisation of monomeric R3 also inhibit the growth of preformed R3 fibrils or dissociate them. R3 was first allowed to assemble for 24 h in the absence of drugs and then polymerise into mature fibrils for 24 additional hours in the absence/presence of drugs.

After 24 h of R3 aggregation, AFM analysis showed the presence of a mixture of smaller protofibrils and granular aggregates, which were highly heterogeneous in morphology (Fig. 2A). A gradual decrease in ThT signal following the addition of drugs at the 24th hour indicated the dissociation of β-sheet-rich structures (Fig. 2B). These findings were verified by AFM analysis of samples collected 24 h after the addition of drugs. There was either a complete dissociation of protofibrils into globular structures by doxorubicin or the presence of a mixture of granules and short fibril-like structures by paclitaxel, cisplatin, resveratrol and quercetin (Fig. 2C). Overall, these data indicate that disaggregation of preformed aggregates is more evident following the addition of doxorubicin.

Mechanisms of drug effect on R3 fibrillisation

Cysteine oxidation of wild-type tau results in the formation of disulfide-bonded dimers, and dimers with intermolecular disulfide bonds are highly prone to aggregation than those with intramolecular disulfide bonds [14]. R3, similar to wild-type three-repeat tau [14], contains a single cysteine residue and forms intermolecular disulfide-bonded dimers [30]. We show that dimers are absent in monomeric samples and only appear when R3 peptide is aggregated under a nonreducing condition (Fig. 3A). This dimer band completely disappears when aggregates are treated with 10% β-mercaptoethanol before loading to gels (Fig. 3A). However, aggregating R3 under a reducing condition (+heparin/+DTT) affected dimerisation as indicated by the decrease in dimer band (Fig. 3A,B). These data suggest that aggregating R3 peptide under reducing conditions inhibits intermolecular disulfide-bonded dimerisation, similar to inhibiting three-repeat tau dimerisation [14]. To determine whether drugs inhibit R3 fibrillisation by affecting dimer formation, we analysed total aggregates and pelleted fractions by nonreducing SDS/PAGE (Fig. 3C,D). The quantification of dimer band intensity indicated that

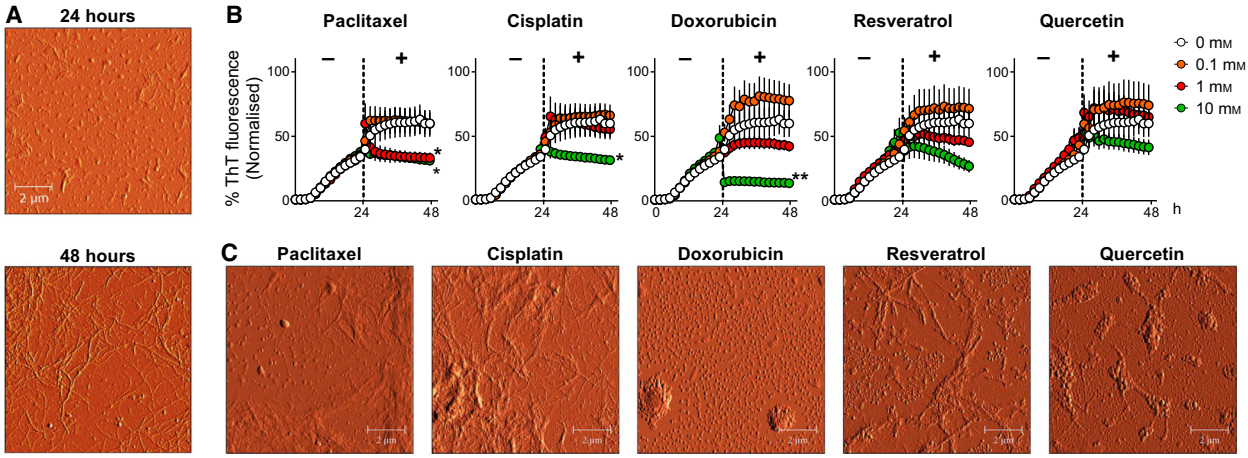

Fig. 2. Inhibition of elongation of preformed R3Ags or protofilaments. (A) AFM images of R3 (proto) fibrils formed after 24 and 48 h of aggregation under nonreducing conditions. (B) Graphs showing the effect of drugs on the elongation of R3 (proto) fibrils. Vertical dotted lines indicate the time at which the drugs were added. Mean ± SEM, $n = 3$ independent experiments. $^{**}P < 0.01$ and $^{*}P < 0.05$ vs 0 μM (control), one-way ANOVA, Dunnett's *post hoc* test. (C) AFM images of R3 fibril morphology after 24 h of incubation in the presence of indicated drugs at 10 μM concentration. See the morphology of drug-untreated fibrils formed after 24 and 48 h of aggregation in panel A.

paclitaxel, doxorubicin, resveratrol and quercetin significantly inhibited dimer formation (Fig. 3E,F).

The Cys322 in R3 is essential for its dimerisation, and the binding of drugs to this site blocks the formation of toxic tau species [14,16]. To determine whether inhibition of R3 dimerisation was due to the binding of drugs to Cys322, we used mutant R3 (R3mut) peptides containing Ala instead of Cys at position 322. Aggregating R3mut peptides under different aggregation conditions indicated that the presence of heparin was essential for aggregation (Fig. S2A), indicating that Cys322, in addition to the hexapeptide sequence, defines the self-aggregation of R3. The Cys-to-Ala substitution only affected the antiaggregation effect of quercetin, but not other drugs (Fig. 3G; Fig S2B). Since R3mut did not dimerise, no effect of drugs was evident on dimerisation (Fig. S2C). The absence of quercetin effect was also evident at a concentration of 10 μM (Fig. S2D). However, oversaturating quercetin concentrations inhibited R3mut aggregation, presumably due to nonspecific binding or because of DMSO (Fig. S2E). DMSO was between 0.01% and 0.1% at 1–10 μM concentrations of all drugs (Fig. 3G; Fig. S2D), and 0.30% and 0.60% at 50 and 100 μM quercetin concentrations, respectively (Fig. S2E).

Overall, these data indicate that quercetin interaction with Cys322 residue results in the abrogation of dimerisation and consequently fibrillisation of R3. The effect of paclitaxel, doxorubicin and resveratrol on R3 dimerisation and fibrillisation results independently of Cys322 residue.

Molecular dynamics simulation of drug–peptide interaction

To gain a deeper insight into the mechanism of antifibrillisation effects of drugs, we performed molecular dynamics (MD) simulations. In the absence of drugs, R3 monomers displayed high flexibility, in agreement with its nonstructured nature. R3 dimer, in the absence of any drugs, was less flexible and preferred an extended β-sheet structure, housing the Cys residue in the loop (Fig. 4A). In the presence of drugs, the dimer became less stable, which is evident by fewer contacts formed between R3 chains, and each drug bound to different regions of the R3 dimer. Paclitaxel interacted directly with the N-terminal of R3 that harbours the aggregation-prone sequence, VQIVYK. Whereas doxorubicin and resveratrol interacted mainly with the C-terminal region, quercetin stayed in contact with C-terminal and Cys residue (Fig. 4B), explaining the absence of quercetin effect on mutant R3 peptide aggregation (Fig. 3E).

Exogenous R3Ag effect on intracellular Tau-RD seeding

Before investigating the effect of drugs on R3Ag-mediated seeding of intracellular tau, we first examined the effect of R3 monomer or R3Ags alone in Tau-RD P301S FRET biosensor cells [26]. R3 monomers did not induce seeding and were nontoxic to cells (Fig. 5A–C). Next, we determined the effect of R3Ags

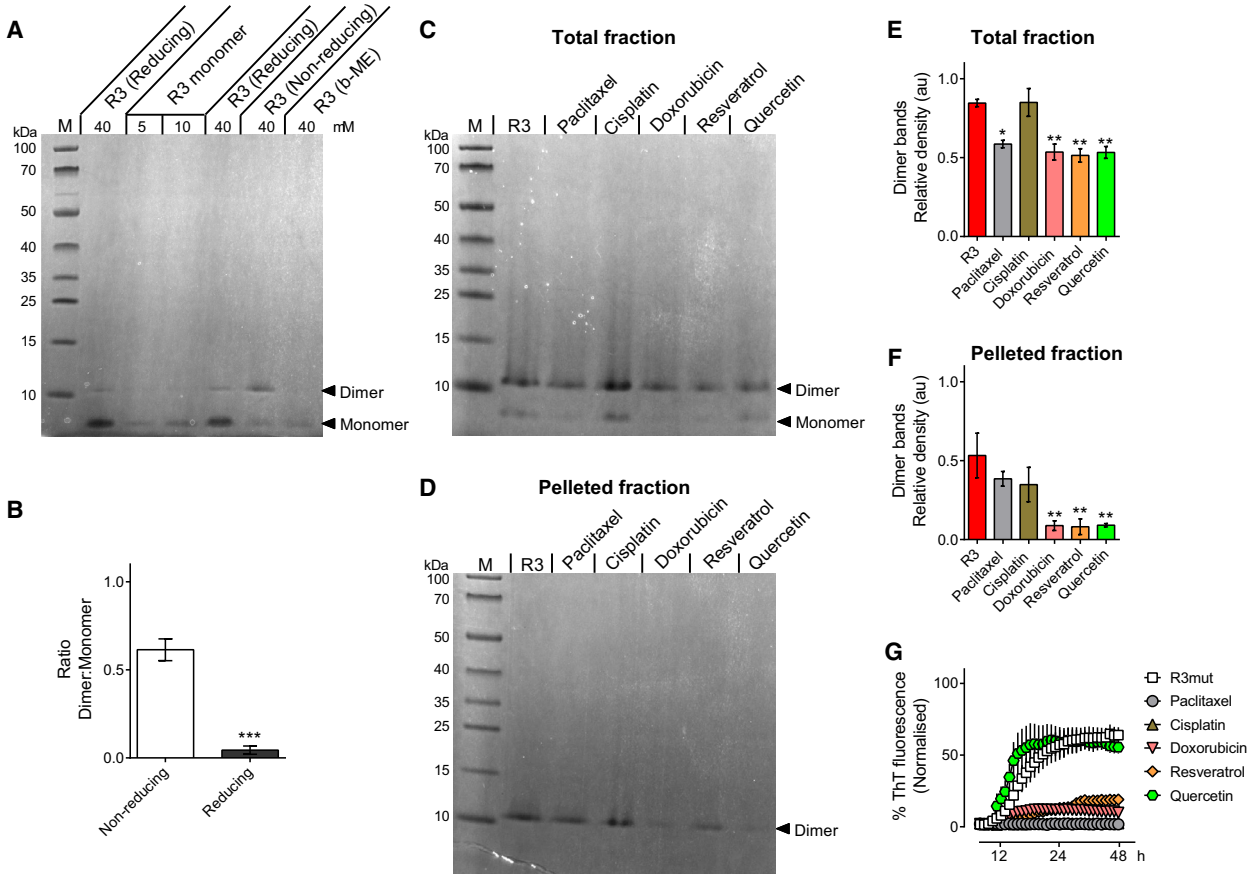

Fig. 3. Drug effect on R3 dimerisation. (A) Representative gel image showing the absence of dimer bands in R3 monomers electrophoresed at two concentrations (5 and 40 μM) and a strong dimerisation of 40-μM R3 under a nonreducing than reducing condition after 48 h of aggregation. The addition of β-ME (β-mercaptoethanol) to R3Ags formed under nonreducing conditions before gel loading abolishes the dimer band. $n = 3$–4 independent experiments. M, marker. (B) A comparison of dimer to monomer bands under nonreducing and reducing aggregation. Mean ± SEM, $n = 3$–4 independent experiments, $^{***}P < 0.001$, two-tailed Student's *t*-test, unpaired. (C, D) Gel images showing dimer bands in total (C) and pelleted (D) fractions following R3 aggregation in the absence or presence of the indicated drugs at the 10 μM concentration. M, marker. (E, F) Quantification of dimer band intensities in total (E) and pelleted (F) fractions shown in C and D. Mean ± SEM, $n = 3$ independent experiments, $^{**}P < 0.01$ and $^{*}P < 0.05$ vs R3, one-way ANOVA, Dunnett's *post hoc* test. (G) Aggregation of R3mut peptide in the absence or presence of indicated drugs at a 1 μM concentration under a nonreducing condition. Mean ± SEM, $n = 3$ independent experiments.

with and without sonication. We decided to check the effect of sonicated R3Ags because a recent study showed that smaller soluble aggregates formed after sonication of the fibrils of human Tau-441 have greater seeding activity than nonsonicated fibrils [31]. Although R3Ags, in general, induced seeding, there was no difference in seeding between cells treated with nonsonicated or sonicated R3Ags (Fig. 5A,B). Furthermore, irrespective of sonication, R3Ags were nontoxic to cells when treated for over 72 h (Fig. 5C).

Interestingly, although R3Ags were nontoxic, we observed a significant reduction in the cell number after 72 h of cell treatment with aggregated but not monomeric R3 (Fig. 5D). To check whether R3Ags affected cell growth, we evaluated a time-dependent change in the total cell number (Fig. 5E). Compared with untreated control, there was a significant decrease in the growth of cells treated with R3Ag (Fig. 5E). Monomeric R3 did not affect cell number, and there was no difference between the effect of nonsonicated and sonicated R3Ags on cell number (Fig. 5D,E). Overall, these findings indicate that R3Ags, irrespective of sonication, do not cause cell death by disrupting the cell membrane integrity but induce seeding and significantly reduce cell growth.

To determine whether the decrease in cell growth and seeding is related, we treated cells with sonicated R3Ags premixed with or without Lipofectamine and

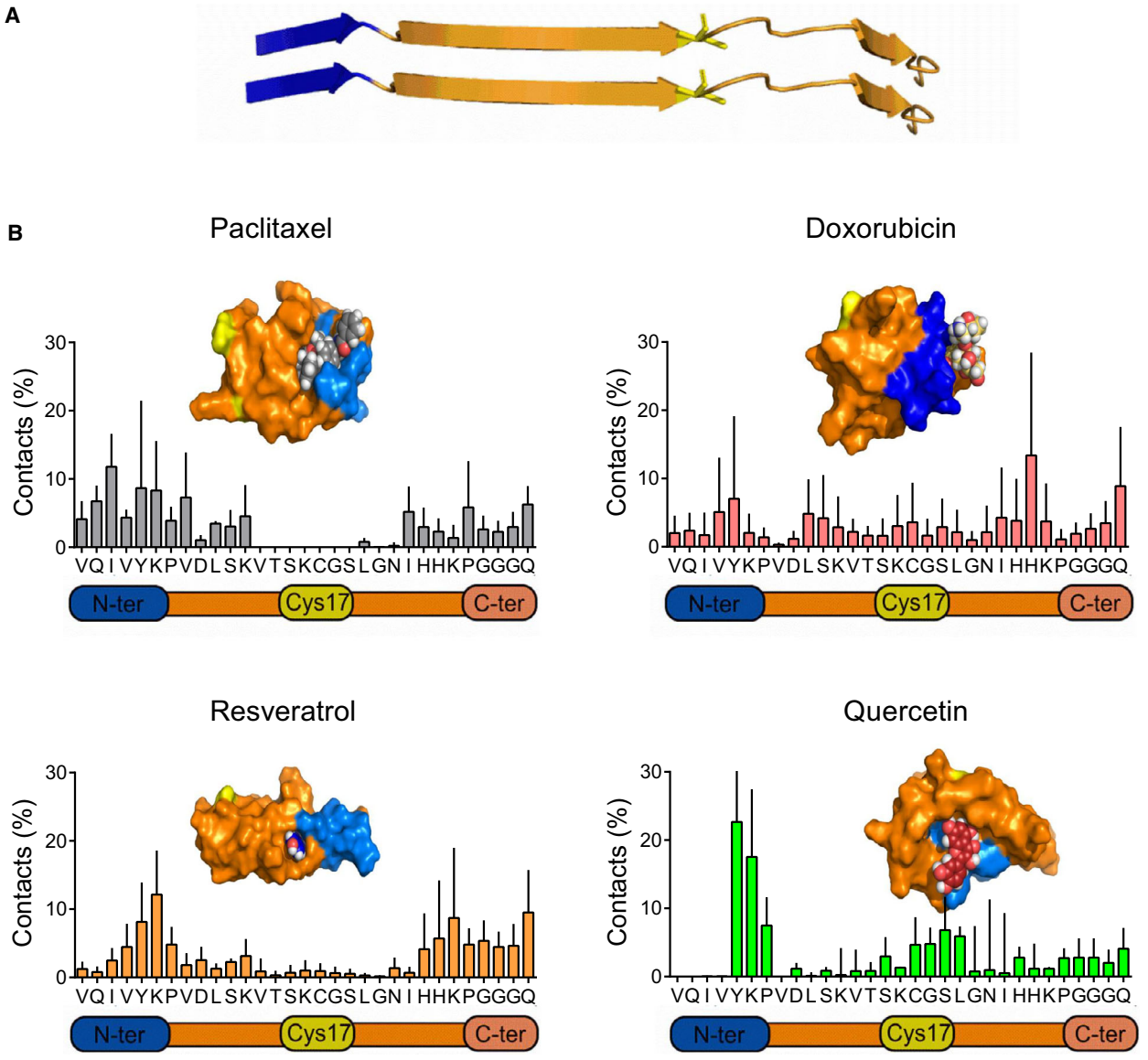

Fig. 4. Molecular dynamics simulation of drugs with R3 dimer. (A) A starting structure of R3 dimer for MD simulations prepared from X-ray structure (PDB ID: 5O3L). Stripes represent β-strands. (B) Graphs show the frequency of paclitaxel contact with N-terminal, doxorubicin and resveratrol with C-terminal, and quercetin with C-terminal and the loop housing Cys residue. Error bars represent standard deviations of contact frequencies. Standard deviations were calculated with the block analysis for four separate blocks ($n = 4$). Inset images show R3 surface (N-terminal part in blue and Cys in yellow) and drugs in sphere models. Reported structures were generated using the PyMOL Molecular Graphics System, Version 2.0, Schrödinger, LLC (New York, NY, USA).

monitored them every 24 h for 72 h by imaging (Fig. 5F). The data show a time-dependent increase in seeding only in cells treated with R3Ags premixed with Lipofectamine (Fig. 5Gi), and correspondingly, these cells show reduced growth over time compared with control cells (Fig. 5Gii). In contrast, cells treated with R3Ags without premixing with Lipofectamine do not show seeding or a decrease in growth (Fig. 5G). Overall, these results indicate that R3Ags do not disrupt the cell membrane and affect cell viability but potentially cause alterations in metabolic activity and cell cycle due to cellular stress from protein aggregation [32,33].

Drug treatment abrogates R3Ag-mediated intracellular tau seeding

The propagation of tau pathology due to seed-competent tau species precedes the formation of NFTs

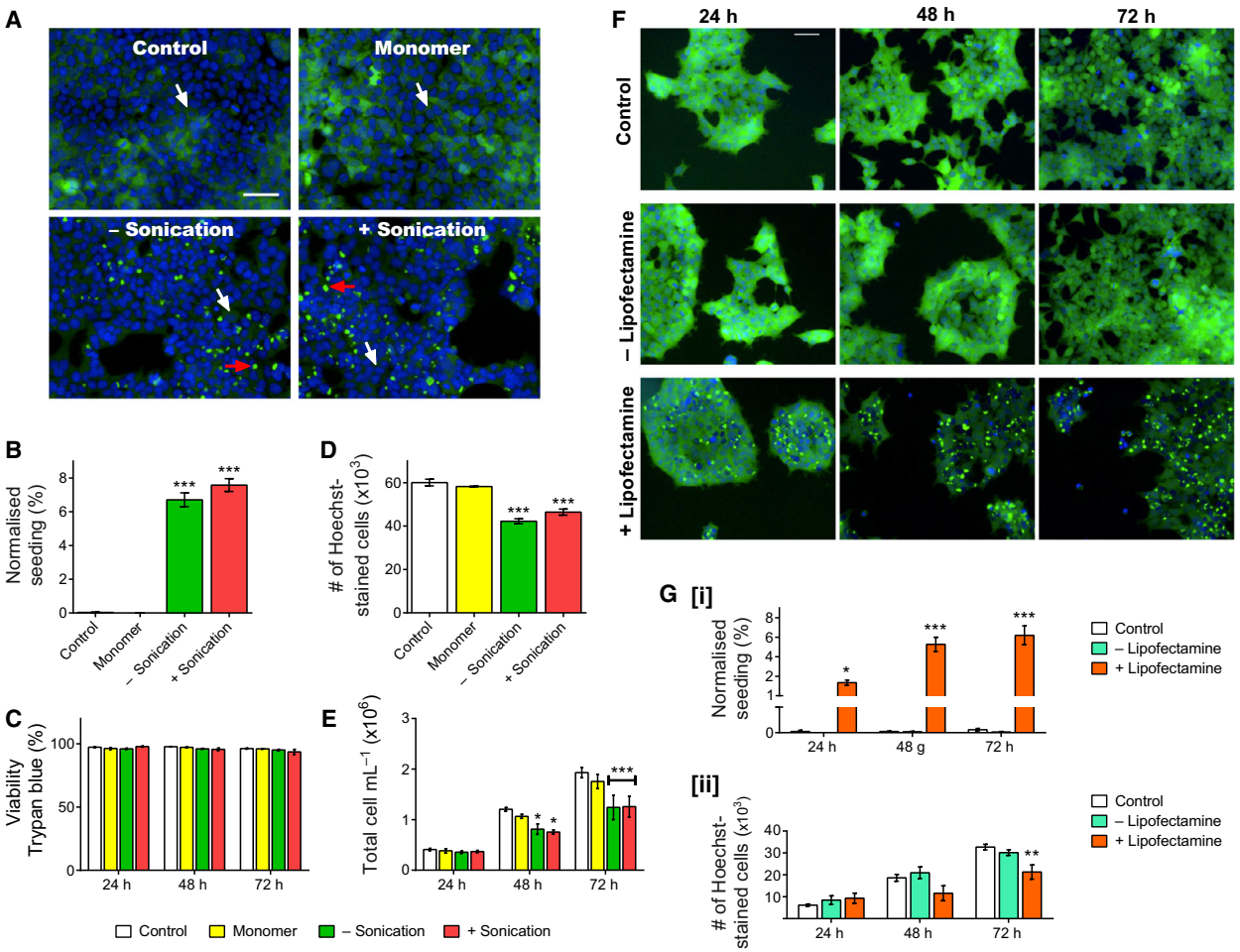

Fig. 5. Effect of R3Ag on seeding and viability. (A) Representative images showing the effect of R3 monomer and nonsonicated (– sonication) and sonicated (+ sonication) R3Ags on seeding after 72 h of treatment. Nuclei are stained blue with Hoechst-33342. Red arrows indicate representative cells containing seeded intracellular Tau-RD aggregates, and white arrows indicate representative cells without aggregated Tau-RD. Scale bar: 50 μm. (B) Quantification of seeding after 72 h of cell treatment with monomeric R3 (monomer), and nonsonicated (– sonication) and sonicated (+ sonication) R3Ags. (C) Cell viability quantified by trypan blue assay after treatment of cells with R3 monomer and nonsonicated and sonicated R3Ags for 24–72 h. (D) Number of Hoechst-stained cells after 72 h of indicated treatment of cells. (E) Time-dependent change in cell growth quantified by trypan blue assay following treatment of cells with R3 monomer and nonsonicated and sonicated R3Ags. Data in B–E are mean ± SEM of 3–4 independent experiments, ***$P < 0.001$, **$P < 0.01$ and *$P < 0.05$ vs control, one-way ANOVA, Tukey's *post hoc* test. (F) Representative images showing a time-dependent effect of R3Ags premixed (+ Lipofectamine) or not premixed (– Lipofectamine) with Lipofectamine transfection reagent on cell density and seeding. Scale bar: 50 μm. (G) Time-dependent increase in seeding (Gi) and decrease in the number of Hoechst-stained cells (Gii) after cell treatment with R3Ags premixed (+ Lipofectamine), but not premixed (– Lipofectamine), with Lipofectamine or control. Data are mean ± SEM of 3 independent experiments, ***$P < 0.001$, **$P < 0.01$ and *$P < 0.05$ vs control in each time-point, two-way ANOVA, Sidak's *post hoc* test.

in AD [2,26]. Therefore, we sought to determine whether pretreating exogenous R3Ags with drugs inhibits the seeding of native tau when introduced in biosensor cells. To this end, we performed two sets of cell treatments as shown in the scheme in Fig. 6A. In the first set (Fig. 6Ai), R3Ags were first incubated (capped) with drugs for 16 h, followed by sonication of capped aggregates before treating cells, as described previously [13]. Alternatively, we first sonicated R3Ags and then capped them with drugs before treating cells (Fig. 6Aii). In the second set, we treated cells directly with R3Ags formed in the absence or presence of drugs, referred to as preinhibited R3Ags (Fig. 6Aiii).

We show that capping R3Ags with resveratrol and quercetin significantly abrogated seeding compared to cells treated with uncapped R3Ags (Fig 6B,C; unnormalised aggregate and cell number are in Fig. S3A,B). While capping with doxorubicin reduced seeding, the

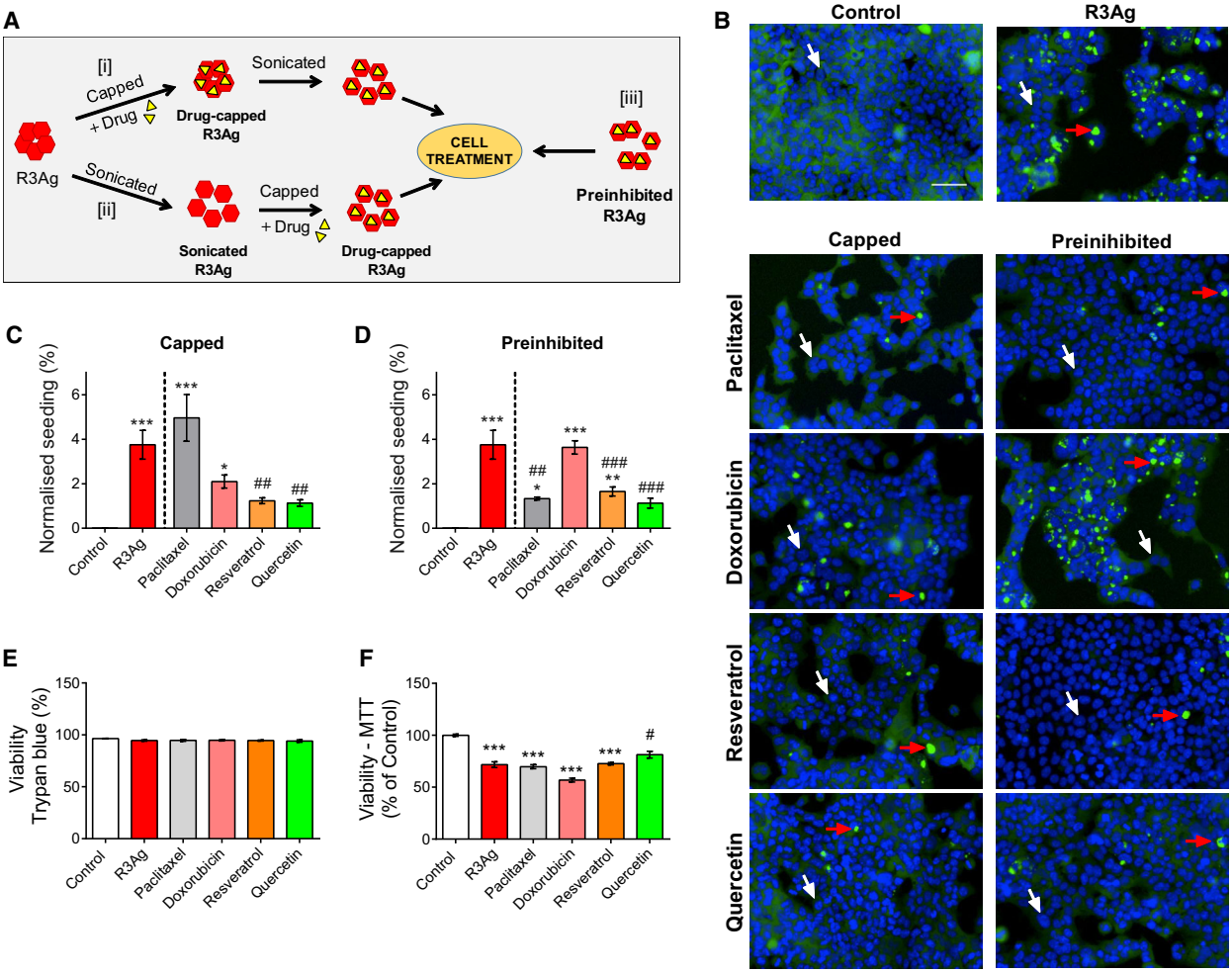

Fig. 6. Drug treatment abrogates seeding-competent R3Ag formation. (A) Schematic representation of the seeding experiments. (B) Representative images show seeding post-72 h in untreated cells (control), and cells treated with R3Ags or R3Ags capped or preinhibited with the indicated drugs. Nuclei are stained blue with Hoechst-33342. Red arrows indicate representative cells containing seeded intracellular Tau-RD aggregates, and white arrows indicate representative cells without aggregated Tau-RD. Scale bar: 50 μm. (C, D) Quantification of seeding following treatment of cells with R3Ag and drug-capped (C) or drug-preinhibited (D) R3Ags for 72 h. Data in C and D are mean ± SEM of $n = 4$–5 independent experiments, $^{***}P < 0.001$, $^{**}P < 0.01$ and $^{*}P < 0.05$ vs control; and $^{\#\#\#}P < 0.001$, $^{\#\#}P < 0.01$ and $^{\#}P < 0.05$ vs R3Ag, one-way ANOVA, Tukey's *post hoc* test. Raw data showing unnormalised aggregate and cell numbers are shown in Fig. S3A, B. (E, F) Viability of cells measured by trypan blue (E) and MTT (F) assays following treatment with drug-untreated R3Ags and drug-preinhibited R3Ags for 72 h. Data are mean ± SEM, $n = 3$, $^{***}P < 0.001$ and $^{**}P < 0.01$ vs control; and $^{\#}P < 0.05$ vs R3Ag, one-way ANOVA, Tukey's *post hoc* test.

difference was insignificant (Fig 6C). Interestingly, sonicating resveratrol or quercetin-capped R3Ag abolished the protective effect conferred by the drugs on Tau-RD seeding (Fig S3C). Similarly, cells treated with preinhibited R3Ags formed in the presence of paclitaxel, resveratrol and quercetin were significantly less active in seeding the aggregation of Tau-RD in cells (Fig. 6B,D). None of the drugs at their final concentrations (paclitaxel 5 nM, doxorubicin 50 nM, and resveratrol and quercetin 200 nM), when administered alone, induced seeding (Fig. S3D) or affected the viability of cells (Fig. S3E).

Our data from AFM analysis of drug-preinhibited R3Ags after 48 h of aggregation assay had shown the formation of a heterogeneous mixture of aggregates, particularly in the presence of doxorubicin (Fig 1D). To check whether these globular assemblies formed in the presence of drugs are toxic, we treated cells with preinhibited R3Ags for 72 h and analysed cell viability by trypan blue exclusion and MTT assays. The trypan

blue assay showed no change in viability following treatment with R3Ag or preinhibited R3Ags (Fig. 6E), indicating the absence of cell membrane perturbation. However, preinhibited R3Ags could not reverse the reduced cell growth compared with control cells (Fig. S3F). Except for doxorubicin (50 nM), none of the other drugs at their final concentrations (paclitaxel 5 nM, and resveratrol and quercetin 200 nM) inhibited cell growth compared with control cells (Fig. S3F).

Intriguingly, the MTT assay indicated a significant reduction in viability upon cell treatment with R3Ags and only preinhibited aggregates formed in the presence of quercetin improved viability compared with R3Ag-treated cells (Fig. 6F). Except for doxorubicin, paclitaxel, resveratrol and quercetin on their own did not affect cell viability, as quantified by MTT assay (Fig. S3G). These data indicate that although aggregates do not disrupt the cell membrane, R3Ags affect the metabolic activity of cells, as indicated by the MTT assay. Quercetin abolished the formation of toxic R3 species and improved the viability of cells compared to cells treated with only R3Ags.

So far, our data indicated that the tested drugs prevent the formation of seeding-competent R3Ags *in vitro*. To show whether drugs prevented seeding activity in cells, we pretreated cells with drugs for 2 and 24 h and then exposed them to either aggregation buffer or R3Ags for an additional 24 h (Fig. 7A). We show that pretreating with all drugs for 2 h (Fig. 7B) or paclitaxel, resveratrol and quercetin for 24 h (Fig. 7C) protected cells against R3Ag-mediated seeding. The quantification of the cell number by imaging indicated no statistically significant effect of drugs or R3Ag (Fig. S4).

Drugs protect *C. elegans* from R3Ags-mediated toxicity

We used *C. elegans* as a versatile *in vivo* model to evaluate the toxicity of R3Ags with or without drug treatment [35,36]. Drug-capped and drug-preinhibited R3Ags were administered to worms for 2 h, and the pharyngeal pumping was scored after an additional 2–24 h to determine whether the drug treatment affected aggregate-mediated toxicity *in vivo* (Fig. 8A). The administration of aggregation buffer (vehicle) alone did not cause any modification of the pharyngeal motility compared with worms fed with 1× phosphate-buffered saline (PBS; pH 7.4) (Fig. S5). However, 2 h after the administration of R3Ags, but not monomeric R3, a severe pharyngeal dysfunction was observed compared to nematodes fed with vehicle (Fig. S5). Interestingly, the pharyngeal impairment caused by R3Ags is transient, as indicated by the absence of toxicity 24 h after administration (Fig. S5). These results indicate that R3 monomers are nontoxic *in vitro* in cells (Fig. 5C) and *in vivo* in *C. elegans*.

Capping-preformed R3Ags with paclitaxel and quercetin, but not resveratrol, significantly protected worms from the toxicity of R3Ags scored 2 h after the administration (Fig. 8B; Table 3). R3Ags formed in the presence of paclitaxel, resveratrol or quercetin resulted in less toxicity than R3Ags (Fig. 8C; Table 3). In both capping and preinhibiting experiments, the effect of drugs alone was also considered by feeding worms with the final concentration of drugs. However, paclitaxel and resveratrol caused a minor but significant reduction of the pharyngeal function in preinhibited experiments (Fig. 8C); they exerted a significant protective effect against R3Ag toxicity (Table 3).

Although the above findings indicate that capping or preinhibiting with drugs reverses the toxicity of R3Ags, the mechanisms underlying this protection remained unanswered. To this end, we first pretreated worms with nontoxic concentrations of paclitaxel, resveratrol and quercetin for 24 h and then administered them with either aggregation buffer or R3Ags for 2 h, as shown in the scheme (Fig. 8D). Similar to what was observed in the previous experimental conditions, R3Ags significantly reduced the pharyngeal pumping rate in worms compared to those fed with aggregation buffer (Fig. 8E). Thus, the pretreatment of worms with paclitaxel, resveratrol and quercetin for 24 h offered a significant protective effect, making worms less susceptible to R3Ag toxicity (Fig. 8E; Table 3).

Discussion

There is strong support for repurposing approved and experimental or investigational oncology drugs for AD therapy [37,38]. Although the precise mechanisms remain elusive, different drugs may target various pathways, consequently protecting neurons against degeneration. For example, tamoxifen acts as an oestrogen-like agonist to enhance cholinergic and hippocampal activities, improving cognitive functions and reducing dementia risk in older women [39]. Taxanes restore the damaged microtubule networks caused by tau loss of function, improving motor and cognitive functions in AD transgenic mice [40]. Sunitinib has antiacetylcholinesterase activity and attenuates cognitive impairments in AD mice, similar to donepezil [41]. Bexarotene clears amyloids from AD mouse brains [42], although, in later studies, it was not effective in AD treatment or prevention [43]. Carmustine and imatinib reduce the Aβ plaque burden by preventing

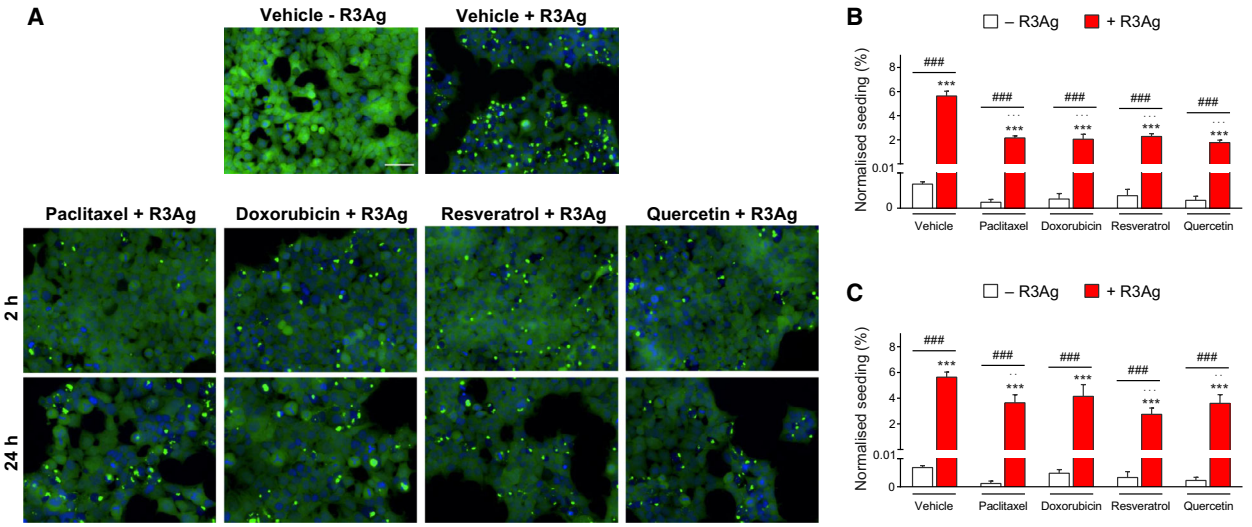

Fig. 7. Drug pretreatment of cells prevents seeding by exogenous R3Ags. (A) Representative images showing pretreatment with paclitaxel, doxorubicin, resveratrol or quercetin for either 2 or 24 h, but not aggregation buffer (vehicle), protects cells from seeding by R3Ag. Nuclei are stained blue with Hoechst-33342. Scale bar: 50 μm. (B, C) Quantification of seeding after cell treatment with aggregation buffer (vehicle), paclitaxel (1 nM), doxorubicin (10 nM), resveratrol (200 nM) or quercetin (200 nM) for either 2 h (B) or 24 h (C) followed (red bars, + R3Ag) or not followed (white bars, – R3Ag) by R3Ag. Data are mean ± SEM of $n = 3$ independent experiments, $^{***}P < 0.001$ vs vehicle – R3Ag; $^{\cdots}P < 0.001$ and $^{\cdot\cdot}P < 0.01$ vs vehicle + R3Ag; and $^{\#\#\#}P < 0.001$, – R3Ag vs + R3Ag, two-way ANOVA, Bonferroni's *post hoc* test.

altered processing of Aβ-precursor protein [44,45] and AD-specific tau phosphorylation [45]. Similarly, lonafarnib activates tau aggregate clearance via lysosomes, reducing tau pathology and behavioural abnormalities in AD mice [46].

We used peptides of R3 to test our hypothesis that antitumour drugs may prevent the formation of prion-like seeds by inhibiting the nucleation-dependent tau aggregation. Our data revealed that the addition of paclitaxel, docetaxel, cisplatin, doxorubicin, daunorubicin, resveratrol and quercetin effectively inhibited the *in vitro* fibrillisation of R3 peptides into β-sheet-rich aggregates (Fig. 1C; Fig. S1A). The antifibrillisation effect of drugs was further validated by Congo red dye and microscopic analysis of aggregates formed in the presence of drugs (Fig. 1D,E; Fig. S1D). These validation studies also ruled out the plausibility that the antifibrillisation effects of resveratrol and quercetin were due to the competitive interaction with ThT for binding to fibrils. In addition to inhibiting fibrillisation, these drugs also caused a complete-to-partial disaggregation of preformed fibrils (Fig. 2). The ability of drugs to disaggregate preformed fibrils is an important feature given the presence of pre-existing aggregates in the brain when patients are diagnosed with AD.

The antifibrillisation effect of paclitaxel, doxorubicin, resveratrol, and quercetin resulted from the inhibition of R3 dimerisation (Fig. 3C,D). Furthermore, we showed that the presence of Cys in the R3 was essential for the antifibrillisation effect of quercetin since R3mut, with a Cys-to-Ala substitution, continued to aggregate in the presence of optimal concentrations of quercetin (Fig. 3E; Fig. S2C–E). These findings were substantiated by MD simulation studies that showed the interaction of paclitaxel with the N-terminal VQIVYK sequence that plays a prominent role in self-aggregation of R3 [10], and quercetin with Cys residue, involved in peptide dimerisation [16] (Fig. 4). Additionally, it appears that interaction with the C-terminal of R3 by doxorubicin and resveratrol also prevents dimerisation. Overall, the findings suggest that the drugs potentially trap R3 monomers or assembly-competent intermediate aggregates, affecting the dynamic equilibrium of R3 fibrillation [47].

Previous studies have demonstrated that fibrils are generally nontoxic to cells [48,49]; rather, oligomeric forms affect viability by disrupting the cell membrane [50]. In agreement, we show that R3Ags do not affect the viability of cells by disruption of the cell membrane (Fig. 5C). However, R3Ag-mediated seeding of intracellular tau reduces the growth of the seeded cells (Fig. 5E). The limited growth is related to the intracellular accumulation of Tau-RD aggregates, as indicated by the absence of seeding or cell growth inhibition in cells treated with R3Ags in the absence of Lipofectamine (Fig. 5G, green columns). Cells with intracellular NFTs or expressing aggregated proteins have been

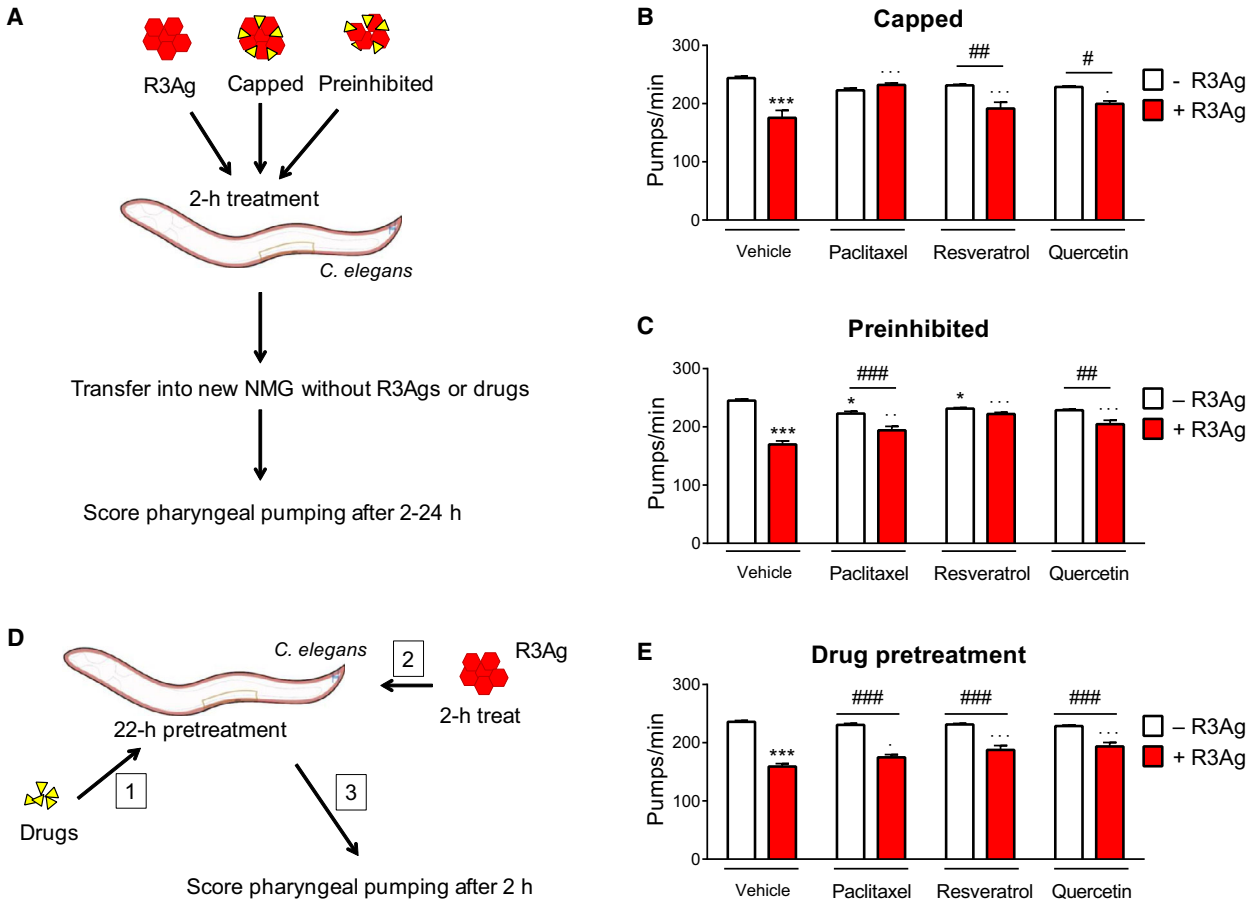

Fig. 8. Drug treatment reverses the toxicity of R3Ags in *C. elegans*. (A) Schematic representation of experimental set-up showing the feeding of *C. elegans* with R3Ags, drug-capped R3Ags or drug-preinhibited R3Ags. (B, C) Effect of R3Ags administered alone (vehicle) and drug-capped R3Ags (B) or drug-preinhibited R3Ags with 5 nM paclitaxel, 200 nM resveratrol or 200 nM quercetin (C) on pharyngeal function scored 2 h after administration (red bars, + R3Ag). The effect of aggregation buffer (vehicle) and 5 nM paclitaxel, 200 nM resveratrol or 200 nM quercetin was also evaluated (white bars, – R3Ag). (D) Schematic representation of experimental set-up showing the pretreatment of worms for 24 h with drugs or aggregation buffer (Vehicle) [1] followed by exposure to R3Ags for 2 h [2] and scoring of pharyngeal pumping post-2 h [3]. (E) Effect of aggregation buffer (vehicle), 5 nM paclitaxel, 200 nM resveratrol or 200 nM quercetin followed (red bars, + R3Ag) or not followed (white bars, – R3Ag) by the administration of R3Ags on the pharyngeal pumping. Data in B, C and E are mean ± SEM, $n = 30$, $^{***}P < 0.001$ and $^{*}P < 0.05$ vs vehicle – R3Ag; $^{\dddot{}}P < 0.001$, $^{\ddot{}}P < 0.01$ and $^{\dot{}}P < 0.05$ vs vehicle + R3Ag; and $^{\#\#\#}P < 0.001$, $^{\#\#}P < 0.01$ and $^{\#}P < 0.05$ – R3Ag vs + R3Ag, two-way ANOVA, Bonferroni's *post hoc* test.

reported to have an aberrant cell cycle or proliferate slowly than control cells [32,33].

Next, we demonstrated that the seeding competency of R3Ags is inhibited following capping with resveratrol and quercetin (Fig. 6B,C). Further, R3Ags formed in the presence of paclitaxel, resveratrol and quercetin are significantly less competent in seeding native Tau-RD (Fig. 6B,D), and these preinhibited R3Ags seem to have no additional effect on cell viability (Fig. 6E). However, although the drugs prevented seeding by R3Ags, they could not revert the limited cell growth (Fig. S3F). Interestingly, quercetin reversed the effect of R3Ags on the metabolic activity and thus the viability of cells, as quantified by the MTT assay (Fig. 6F). Cells with tau pathology display a senescence-like phenotype [32]. Given the senolytic activity of quercetin [51], it could have improved metabolic functions, reversing the senescence-like phenotype. However, future studies are needed to test this speculation.

In addition to abrogating the formation of seeding-competent fibril *in vitro* (Fig. 6), the drugs also inhibited the seeding activity in cells. This was indicated following pretreatment of cells with drugs followed by exposure to seeding-competent R3Ags (Fig. 7), suggesting that the drugs prevented the addition of monomers (intracellular P301S) to seeds (R3Ags) possibly by inhibiting template-assisted filament growth [34] that

Table 3. *P*-value summary from Fig. 8. *P*-values of the interaction obtained from the two-way ANOVA and Bonferroni's *post hoc* analysis performed on data from the different experiments shown in Fig. 6, proving the protective effect exerted by some drugs on the R3Ag toxicity.

	Two-way ANOVA interaction (*P*-values)		
	Drug-capped R3Ag	Drug-preinhibited R3Ag	Drug pretreatment before R3Ag
Paclitaxel	< 0.001	< 0.001	0.039
Resveratrol	Not significant	< 0.001	0.002
Quercetin	0.010	< 0.001	< 0.001

inhibited the aggregation of intracellular tau. Like other amyloidogenic proteins, R3Ags also caused a specific pharyngeal dysfunction in *C. elegans* (Fig. 8). This effect was reverted when the peptide was capped or its aggregation preinhibited with paclitaxel, resveratrol or quercetin, indicating that these drugs can mask residues relevant for the R3Ag proteotoxicity in *in vivo* proteins [35]. Together with findings from *in vitro* assay, these data indicate that the drugs inhibited the primary nucleation of R3 fibrillisation that initiates the production of toxic R3 species, a process similar to inhibiting toxic $A\beta_{42}$ generation by bexarotene [12].

Alzheimer's disease is a dual proteinopathy of tau and Aβ proteins that act alone or in combination in the process of neurodegeneration [3]. A deeper understanding of how pathogenic seeds form and drive distinct structural polymorphs in tau spreading may reveal new insights for designing treatment strategies. A study using P301S Tg mice has shown that the intracellular and extracellular tau levels are related, and low levels of extracellular tau may mediate tau pathology [52]. Despite the low concentrations, cells could take up extracellular tau, inducing intracellular tau aggregation and spreading. Several forms of pathogenic extracellular tau, either free or vesicle enclosed, are suspected of spreading tau pathology [Reviewed in Ref. 53]. Therefore, therapeutic interventions, such as immunotherapy or small molecules that target extracellular tau, may halt disease progression. Like any model system, our study also has its inherent weaknesses. Although we have used simple models in our study, our findings present a rational approach for targeting the VQIVYK or cysteine that may block the nucleation-dependent tau aggregation and prion seed generation. We conclude that earlier detection of seed-competent tau inclusions in brains of AD or susceptible patients and targeting these inclusions may prevent or slow tau spreading.

Materials and methods

Chemicals and reagents

All chemicals, unless described otherwise, were purchased from Sigma-Aldrich (St. Louis, MA, USA). Paclitaxel, vincristine sulfate, bleomycin, resveratrol, polydatin, genistein and quercetin were purchased from Sigma-Aldrich and dissolved in DMSO to make a 10-mM stock. All other drugs were obtained from the University Hospital Olomouc (Table 4). The drugs directly from injection vials or 10-mM DMSO stocks were reconstituted in 1× PBS (pH 7.2) to make fresh 1-mM intermediate stock before each experiment. The intermediate stock was then used for making working stocks for all experiments. The final concentration of solvent is listed in Table 4.

Peptide synthesis

R3 peptides were synthesised by solid-phase chemistry using fluorenylmethyloxycarbonyl chloride group (Fmoc)-protected amino acid, with Initiator+Alstra peptide synthesiser (Biotage, Uppsala, Sweden) at 0.1 mM scale on TGA resin. Fmoc deprotection was performed automatically at room temperature by treating the peptide/resin with 20% piperidine in DMF (dimethylformamide) for 3 min, followed by another cycle of 10 min and 4× DMF washes. Amino acids were activated using DIC (N,N′-diisopropylcarbodiimide) and Oxyma Pure, both at 0.5 mM in DMF. R3 peptides were cleaved from the resin with TFA (trifluoroacetic acid): triisopropylsilane solution (95 : 5 vol/vol), precipitated and washed with cold diethyl ether. Purification of crude peptides was carried out in reverse phase HPLC using a semipreparative C4 column (Symmetry 300, Waters, Milford, MA, USA), with mobile phases of 0.1% TFA in water (eluent A)/0.08% TFA in acetonitrile (eluent B) and a linear gradient from 5 up to 100% of eluent B in 60 min. The peaks were collected and characterised by matrix-assisted laser desorption/ionisation time-of-flight (MALDI-TOF) mass spectrometry using an Applied Biosystems (ABI) 4800 MALDI-TOF/TOF Analyzer (Foster City, CA, USA), operating in reflector mode. Solutions containing the peptides with a purity > 95% were finally frozen and dried, and the powders were stored at −20 °C until use. The Fmoc-amino acid and reagents used for peptide synthesis were obtained from Sigma-Aldrich company.

Lyophilised peptides were dissolved in a 0.22-μm syringe filter (Merck Millipore, Burlington, MA, USA)/sterilised deionised water, aliquoted into smaller working stocks and stored at −80 °C. Each working stock underwent a maximum of 2 freeze–thaw cycles.

Aggregation assay and drug testing

The aggregation of R3 peptide was monitored by an *in vitro* ThT binding assay. The peptide solution stored at −80 °C was thawed on ice and centrifuged at 11 300 ***g*** for

Table 4. Source of antitumour drugs and solvent concentrations.

				Vehicle concentration (%) in drug dilutions			
				Intermediate (in 1× PBS)	Final (in 1× PBS)		
	Source	Actual concentration ($mg \cdot mL^{-1}$)	Conversion to mM	1 mM	10 μM	1 μM	0.1 μM
Paclitaxel	Sigma-Aldrich (Cat. No.: T7191)	8.54	10.00	10.00	0.100	0.010	0.001
Docetaxel	University Hospital Olomouc	10	12.38	8.08	0.080	0.008	0.001
Vincristine sulfate	Sigma-Aldrich (Cat. No.: V8879)	5	5.42	18.45	0.184	0.018	0.001
Vinorelbine tartrate	University Hospital Olomouc	10	12.84	7.78	0.080	0.008	0.001
Cisplatin	University Hospital Olomouc	1	3.33	30.03	0.300	0.030	0.003
Oxaliplatin	University Hospital Olomouc	5	12.58	7.95	0.080	0.008	0.001
Carboplatin	University Hospital Olomouc	10	26.94	3.72	0.040	0.004	< 0.001
Cyclophosphamide monohydrate	University Hospital Olomouc	20	76.60	1.31	0.010	0.001	< 0.001
5-Fluorouracil	University Hospital Olomouc	50	384.38	0.26	< 0.001	< 0.001	< 0.001
Methotrexate	University Hospital Olomouc	50	110.04	0.91	0.010	0.001	< 0.001
Fludarabine phosphate	University Hospital Olomouc	10	27.38	3.65	0.040	0.004	< 0.001
Gemcitabine	University Hospital Olomouc	40	151.97	0.66	0.010	0.001	< 0.001
Doxorubicin hydrochloride	University Hospital Olomouc	2	3.45	28.98	0.280	0.028	0.003
Daunorubicin hydrochloride	University Hospital Olomouc	5	9.48	10.55	0.110	0.011	0.001
Bleomycin	Sigma-Aldrich (Cat. No.: B7216)	10	7.06	14.16	0.141	0.014	0.001
Mitomycin C	University Hospital Olomouc	2	5.98	16.72	0.170	0.017	0.002
Irinotecan hydrochloride Trihydrate	University Hospital Olomouc	20	29.54	3.39	0.030	0.003	< 0.001
Etoposide	University Hospital Olomouc	20	33.98	2.94	0.029	0.003	< 0.001
Mitoxantrone	University Hospital Olomouc	6	13.50	7.41	0.070	0.007	0.001
Topotecan hydrochloride	University Hospital Olomouc	1	2.2	45.45	0.450	0.045	0.005
Resveratrol	Sigma-Aldrich (Cat. No.: R5010)	16.24	71.13	1.41	0.010	0.001	< 0.001
Polydatin	Sigma-Aldrich (Cat. No.: 15721)	3.04	7.79	12.84	0.130	0.013	0.001
Genistein	Sigma-Aldrich (Cat. No.: G6649)	2.70	10.00	10.00	0.100	0.010	0.001
Quercetin	Sigma-Aldrich (Cat. No.: Q4951)	4.70	15.55	6.43	0.060	0.006	0.001

45 s on a benchtop centrifuge. A reaction mixture containing 20 μM peptide, 5 μM heparin and 15 μM ThT was prepared in peptide aggregation buffer [20 mM Tris (pH 7.4), 100 mM NaCl, 1 mM EDTA] in an ice-chilled 1.5-mL Eppendorf tube. The reaction mixture was then dispensed into a black, clear-bottom CellCarrier 384-well assay plate

(PerkinElmer, Waltham, MA, USA), followed by sealing the plate with a TopSeal-A PLUS Clear Adhesive Seal (PerkinElmer) to prevent evaporation. Throughout sample preparation, the reagents and assay plate were kept on ice. Following the addition of reagents, the assay plate was placed in an EnSpire Multimode Plate Reader (PerkinElmer), with the temperature of the measurement chamber set to 37 °C. To prevent condensation in the sealed plate, the upper heater temperature was set to 2 °C warmer than the lower heater temperature. The plate reader was set to maintain the assay plate under constant agitation (1000 rpm) during the resting period. The fluorescence of ThT binding (λexc = 460–490 nm, λem = 500–550 nm) to aggregated peptide was recorded every 5 min up to 48 h. For normalised ThT fluorescence plots, the raw data (ThT fluorescence) were normalised to the lower and higher relative fluorescence intensity values in the data set using GRAPHPAD PRISM SOFTWARE (version 7; San Diego, CA, USA).

The effect of antitumour drugs on peptide aggregation was determined in a two-step screening assay, which included peptide aggregation in the presence of drugs to identify active inhibitors. To this end, the reaction mixture was spiked with drugs at 1 μM concentration before dispensing into a 384-well assay plate to determine drug effects. To examine the effect of drugs on the polymerisation of preformed R3Ags into mature fibrils, R3 was first aggregated at 37 °C for 24 h in the absence of drugs. The assay plate was then removed from the plate reader to add drugs from intermediate stocks to get the final desired concentration per well (0.1, 1 and 10 μM). The addition of drugs was performed in < 15 min. After adding drugs, the plate was replaced back into the plate reader, and the fluorescence of ThT binding to aggregates was monitored for an additional 24 h.

In all aggregation assays with drugs, control wells received an equal amount of aggregation buffer containing DMSO at a percentage present in drugged wells. Unless otherwise mentioned, the final concentration of drug solvent was always below 0.5%. All drug treatments were performed in duplicates per plate, and the assay was repeated at least 3 independent times. Note that all peptide aggregation assays in the presence or absence of drugs were carried out for cell and worm treatment experiments in the absence of ThT.

Coomassie gel staining

Peptide aggregates collected after the end of aggregation assay were centrifuged at 21 000 ***g*** on a benchtop centrifuge for 30 min at 4 °C to pelleted insoluble fractions. In addition to noncentrifuged total fractions, the insoluble fractions were mixed with NuPAGE™ LDS Sample Buffer (Thermo Fisher Scientific, Waltham, CA, USA) without reducing agent and boiled for 5 min at 70 °C. The insoluble fractions were mixed with 10% β-ME in LDS Sample Buffer before boiling to denature disulfide bonds. The total and insoluble fractions were electrophoresed using NuPAGE™ 4–12% Bis-Tris protein gels (Thermo Fisher Scientific) at 200 V for 40 min at room temperature in 1× NuPAGE™ MES SDS Running Buffer (Thermo Fisher Scientific). Gels were fixed in a fixative solution [50% methanol (v/v) and 10% acetic acid (v/v) in deionised water] for 30 min and stained with Coomassie Brilliant Blue R-250 staining solution (Bio-Rad, Hercules, CA, USA) for 12 h at 4 °C. Gels were destained by washing multiple times in deionised water, and images of gels were acquired in a ChemiDoc MP imaging system (Bio-Rad).

Atomic force microscopy, fluorescence imagining and Congo red absorbance

For atomic force microscopy (AFM) analysis, collected samples were added dropwise onto a freshly cleaved 10 mm-sized AFM mica disc (Ted Pella, Inc., Redding, CA, USA) and air-dried for 10 min at room temperature. The mica discs were then washed 5× times with a 0.22-μm sterile syringe filter (Merck Millipore)-sterilised deionised water and dried for 10–15 min at room temperature. The discs were strapped on a glass slide using a transparent cello tape to prevent the discs from moving during imaging on an Olympus IX81/Veeco BioScope™ Catalyst™ Atomic Force Microscope (Bruker, Billerica, CA, USA). The images were acquired using a 10× objective under ambient conditions at a scan rate of 0.7 Hz (line per s) and a peak force amplitude of 150 nm. Antimony-doped silicon cantilever probe with a typical resonant frequency of 150 Hz and spring constant of 5.1 Nm^{-1} were employed, and acquired images were processed in GWYDDION 2.40 freeware [54].

The formation of β-sheet-rich aggregates of peptides in the absence or presence of drugs was visualised by staining the content of assay wells with 15 μM ThT after the end of ThT-free aggregation assay and embedding in 0.05% low-melting agarose (Sigma-Aldrich). The images of ThT-stained aggregates were then captured on an Operetta™ high-content screening system (PerkinElmer) using a 2× objective and 488-laser line (λexc = 460–490 nm, λem = 500–550 nm). The captured images were processed using Harmony High-Content Analysis Software (PerkinElmer).

To validate the antifibrillisation effect of drugs, 20 μM R3 was first allowed to fibrillise under a ThT-free proaggregation condition in the absence or presence of drugs at 10 μM concentration in a Spectra 384-well assay plate (PerkinElmer). After 48 h, the contents of the wells were stained with 40 μM Congo red (Sigma-Aldrich), and the absorbance was immediately measured in an EnSpire Multimode Plate Reader (PerkinElmer) at 540-nm wavelength.

Preparation of models for molecular dynamics simulation

Initial structures of monomeric and dimeric R3 peptide (VQIVYKPVDLSKVTSKCGSLGNIHHKPGGGQ) were

cut out from the known crystal structure of multilayered human filament (PDB ID: 5O3L) [55]. The build models were refined according to the native protein sequence (UniProt ID P10636) using Modeller 9.10 homology modelling software to tackle a low resolution of the used X-ray structure [56]. Structures of paclitaxel, resveratrol and quercetin were obtained by ab initio calculations [HF/6-31G(d)] as implemented in GAUSSIAN 09 software [57]. Parameters for molecular dynamics simulations were derived using standard RESP procedure using Antechamber from AMBER 11 package [58] to ensure compatibility with AMBER force fields [59]. The initial structures of R3 with bound ligands were obtained by molecular docking. Structures of paclitaxel, resveratrol and quercetin for docking were prepared using MARVIN 5.10 (http://www.chemaxon.com). The AUTODOCK VINA program was used for docking ligands into the grid box centred at the structure of R3 [60]. The models were immersed in the rectangular box of at least $7 \times 7 \times 7$ nm, and solvated with TIP3P water models, and Na^+ and Cl^- counterions were added to mimic the physiological concentration of 0.15 mol·L^{-1}.

Molecular dynamics procedure

All simulations were carried out with AMBER16 software using the GPU-PMEMD algorithm [58]. The ff14SB force field was used for both drug and peptide [61]. All simulations were subjected to 100 000 steps of steepest descent energy minimisation followed by 5-ns-long thermalisation of solvent and ions. The final production run was set to 1000 ns with a 2-fs-long time step. Bonds involving hydrogens were restrained using the SHAKE algorithm [62]. The temperature was kept constant at 310 K with Langevin dynamics with a collision frequency of 1 ps [63]. The constant pressure of 1 atm was maintained using the Berendsen algorithm at isotropic position scaling [64]. Real-space electrostatics and van der Waals interactions were computed up to 1.0-nm distance. Long-range interactions were treated with the PME algorithm [65]. Periodic boundary conditions were set in all directions, and analyses were performed using the '*cpptraj*' tool from Amber16. Clustering analysis was performed using a density-based DBSCAN clustering method with a 0.9 Å cut-off distance for forming clusters [66]. Protein–drug contacts were calculated using the 'nativecontacts' tool implemented in 'cpptraj' with a 5 Å distance threshold.

Cell culture

Tau-RD P301S FRET Biosensor cells were purchased from ATCC (Manassas, VA, USA) and cultured in DMEM (Gibco, Waltham, MA, USA) supplemented with 10% fetal bovine serum (FBS; Capricorn Scientific GmbH, Ebsdorfergrund, Germany), 1 mM glutaMAX (Gibco) and 1× penicillin–streptomycin solution (Gibco). Cells were maintained in a standard humidified 5% CO_2/atmospheric air incubator at 37 °C. The cells were routinely tested for bacterial, fungal and mycoplasma contaminations and authenticated biweekly or monthly.

Cytotoxicity assay

R3 was assembled under a ThT-free proaggregation condition in the absence/presence of drugs for 48 h. The untreated/preinhibited R3Ags were collected and diluted in 50 µL Opti-MEM (Cat. # 11058021, Thermo Fisher Scientific) containing 1% Lipofectamine LTX (Cat. # 15338100, Thermo Fisher Scientific) and 0.5% Lipofectamine Plus (Cat. # 15338100, Thermo Fisher Scientific). The mixture was incubated for 15 min at room temperature. These transfectants were then added to cells plated in a standard 24- or 96-well plate (Techno Plastic Products AG, Trasadingen, Switzerland) at a density of 0.1×10^6 cells·mL^{-1}. Cell viability was analysed after 72 h of treatment using a standard MTT assay or trypan blue exclusion assay. Cell viability and the cell number and viability by trypan blue assay were measured using a Vi-CELL™ XR Cell Viability Analyser (Beckman Coulter, Brea, CA, USA) following the manufacturer's instructions.

Tau seeding assay

Tau-RD P301S FRET Biosensor cells were plated in a black, clear-bottom CellCarrier 96-well plate (PerkinElmer) at a density of 5×10^4 cells·mL^{-1} in 100 µL of growth medium. The next day, cells were treated with R3 monomers or aggregates premixed in Lipofectamine LTX Plus transfection agent as described below for 72 h.

For seeding assay with drug-capped aggregates, 1 µM fibrillar R3Ags were first incubated with 0.1 µM paclitaxel, 1 µM doxorubicin, and 4 µM resveratrol and quercetin in deionised water for 16 h at 37 °C to make an intermediate stock. Drug-capped fibrils were then sonicated for 1–2 min on a Cup Horn water bath to generate shorter aggregates, as described elsewhere [67], before adding to cells. Alternatively, fibrillar R3Ags (1 µM) were first sonicated and then capped with drugs before adding to cells. The drug-capped aggregates were mixed with 1% Lipofectamine LTX and 0.5% Lipofectamine Plus in Opti-MEM reduced-serum medium and seeded to cells at a ratio of 1 : 1 transfectant to the growth medium. The drug concentrations for capping were chosen based on the concept that drugs required to block seeding by preformed fibrils are about 20 times greater than the amount required to inhibit monomeric tau aggregation [67]. The final concentration of R3Ags was 50 nM, whereas the concentration of paclitaxel was 5 nM, that of doxorubicin was 50 nM, and those of resveratrol and quercetin were 200 nM.

For seeding assay with drug-preinhibited aggregates, 20 µM R3 peptide was first assembled *in vitro* in the presence of 2 µM paclitaxel, 20 µM doxorubicin, and 80 µM resveratrol and quercetin for 48 h. The aggregates formed R3Ags were then diluted into an Opti-MEM to make intermediate

stocks. Five microlitres of intermediate stock of preinhibited R3Ags was then mixed with 1% Lipofectamine LTX and 0.5% Lipofectamine Plus in Opti-MEM and seeded to cells at a 1 : 1 ratio. The final concentration of R3Ags was 50 nM, whereas the concentration of paclitaxel was 5 nM, that of doxorubicin was 50 nM, and those of resveratrol and quercetin were 200 nM.

For drug pretreatment seeding assay, cells were first pretreated with paclitaxel (1 nM), doxorubicin (10 nM), resveratrol (200 nM) and quercetin (200 nM) or just the aggregation buffer for 2 and 24 h at 37 °C. Following drug treatment, cells were washed twice with 1x PBS and then seeded with sonicated R3Ags premixed with 1% Lipofectamine LTX and 0.5% Lipofectamine Plus in Opti-MEM reduced-serum medium and seeded to cells as per the tau seeding assay protocol mentioned above for 24 h.

In all seeding assays, the final concentration of drug solvent (DMSO) per well was always < 0.5%. Control cells were treated with aggregation buffer containing only Lipofectamine LTX Plus transfection agents. All treatments were performed in triplicate per experimental plate, and the experiments were repeated 3–5 independent times.

Quantification of cell number and seeding

Biosensor cells were stained with 10 μM Hoechst-33342 nuclear dye (Invitrogen) for 10–15 min at 37 °C in a humidified incubator prior to imaging. The cells were then washed twice with 1X PBS and replaced with fresh phenol red-free growth medium. Cells were imaged on an Operetta™ High-Content Screening System (PerkinElmer) using a 20× objective, and 488-laser line (λexc = 460–490 nm, λem = 500–550 nm) for CFP/YFP Tau-RD aggregates and 405-laser line (λexc = 360–400 nm, λem = 410–480 nm) for Hoechst-33342. At least 10–12 focal areas were imaged per well of experimental plates. Cell number was quantified by counting Hoechst-stained nuclei, and the seeding was determined by counting the number of intracellular CFP/YFP Tau-RD aggregates using Harmony Image Analysis Software (see Appendix S1). The number of aggregates was then normalised to the total cell number per well, and presented as 'normalised seeding' in our study.

Caenorhabditis elegans studies

Bristol N2 nematodes were obtained from the *C. elegans* Genetic Center (CGC, University of Minnesota, Minneapolis, MN, USA) and propagated at 20 °C on solid Nematode Growth Medium (NGM) seeded with *E. coli* OP50 (CGC) for food as described previously [68]. The effect of R3 monomer and R3Ags on pharyngeal behaviour was investigated by feeding synchronised L3 worms (100 worms/100 μL) with 50 nM monomeric R3 or sonicated R3Ags. Control worms were fed with 1X PBS (pH 7.4) or peptide aggregation buffer (vehicle). Incubation of worms with R3 peptide was performed in the absence of *E. coli* to avoid any potential interference between bacteria and the protein. After 2 h of incubation with orbital shaking at 20 °C, worms were transferred onto NGM plates seeded with OP50 *E. coli*. The pharyngeal pumping rate, measured by counting the number of times the terminal bulb of the pharynx contracted over a 1-min interval (pumps per min), was scored after 2 and 24 h of feeding.

Synchronised L3 worms (100 worms/100 μL) were fed with R3Ags alone, or R3Ags capped with paclitaxel, resveratrol or quercetin for 2 h on orbital shaking at 20 °C to determine the effect of drug-capped R3Ags on pharyngeal function. For determining the effect of preinhibited R3Ags, worms (100 worms/100 μL) were fed with R3 peptides aggregated in the absence or presence of drugs as described in the previous sections. The final concentration of R3Ags fed to the worm was 50 nM, and the concentration of paclitaxel was 5 nM, and concentrations of resveratrol and quercetin were 200 nM. Control worms were fed with the drugs alone or aggregation buffer (vehicle). At the end of incubation, worms were transferred onto NGM plates seeded with OP50 *E. coli*, and the pharyngeal pumping rate was scored 2 and 24 h later.

Alternatively, synchronised L3 nematodes (100 worms/100 μL) were fed with 1 nM paclitaxel, 200 nM resveratrol or 200 nM quercetin to determine whether the pretreatment of worms with antitumour drugs can prevent the proteotoxicity of R3Ags. After 2 h on an orbital shaker at 20 °C, worms were transferred onto NGM plates seeded with OP50 *E. coli* containing the drug at the same concentration. Control worms were transferred onto NGM plates seeded with OP50 without any drugs. After 22 h at 20 °C, 50 nM sonicated R3Ags or the same volume of peptide aggregation buffer were added to each plate, and the pharyngeal pumping rate of worms was scored 2 h later.

Statistical analysis

All statistical analyses were performed using GRAPHPAD PRISM SOFTWARE, and differences were considered significant at $P < 0.05$.

Acknowledgements

The work was supported by the European Regional Development Fund [CZ.02.1.01/0.0/0.0/16_019/0000868 (ENOCH) and CZ.02.1.01/0.0/0.0/16_019/0000754 (Operational Programme Research, Development, and Education)], the Technology Agency of the Czech Republic (TN01000013, PerMed), the Czech Ministry of Education, Youth and Sport (LM2018133), the Internal Student Grant Agency of the Palacký University in Olomouc, Czech Republic (IGA_PrF_2021_031), and the Fondazione Regionale per la Ricerca Biomedica (Care4NeuroRare CP_20/2018). *C. elegans* and

OP50 *E. coli* were provided by the Caenorhabditis Genetics Center (CGC), funded by NIH Office Research Infrastructure Programs (P40 OD010440).

Conflict of interest

The authors declare no conflict of interest.

Author contributions

NA, LM, AB, AC and MR prepared materials, performed the experiments, and analysed and interpreted data. MŠ, KB and MO performed the computational analysis and interpreted the data. NA prepared the first draft of the manuscript. MS, LD, MH and VD critically reviewed the data and wrote the manuscript. VD designed and coordinated the study and revised the manuscript. All authors provided critical feedback and helped shape the research, analysis and manuscript.

Peer Review

The peer review history for this article is available at https://publons.com/publon/10.1111/febs.16270.

References

1 Dujardin S, Commins C, Lathuiliere A, Beerepoot P, Fernandes AR, Kamath TV, De Los Santos MB, Klickstein N, Corjuc DL, Corjuc BT *et al*. (2020) Tau molecular diversity contributes to clinical heterogeneity in Alzheimer's disease. *Nat Med* **26**, 1256–1263.

2 DeVos SL, Corjuc BT, Oakley DH, Nobuhara CK, Bannon RN, Chase A, Commins C, Gonzalez JA, Dooley PM, Frosch MP *et al*. (2018) Synaptic tau seeding precedes tau pathology in human Alzheimer's disease brain. *Front Neurosci* **12**, 267.

3 Vogel JW, Iturria-Medina Y, Strandberg OT, Smith R, Levitis E, Evans AC, Hansson O, Weiner M, Aisen P, Petersen R *et al*. (2020) Spread of pathological tau proteins through communicating neurons in human Alzheimer's disease. *Nat Commun* **11**, 2612.

4 Clavaguera F, Bolmont T, Crowther RA, Abramowski D, Frank S, Probst A, Fraser G, Stalder AK, Beibel M, Staufenbiel M *et al*. (2009) Transmission and spreading of tauopathy in transgenic mouse brain. *Nat Cell Biol* **11**, 909–913.

5 Kaufman SK, Del Tredici K, Thomas TL, Braak H & Diamond MI (2018) Tau seeding activity begins in the transentorhinal/entorhinal regions and anticipates phospho-tau pathology in Alzheimer's disease and PART. *Acta Neuropathol* **136**, 57–67.

6 Ossenkoppele R, Iaccarino L, Schonhaut DR, Brown JA, La Joie R, O'Neil JP, Janabi M, Baker SL, Kramer JH, Gorno-Tempini M-L *et al*. (2019) Tau covariance patterns in Alzheimer's disease patients match intrinsic connectivity networks in the healthy brain. *Neuroimage Clin* **23**, 101848.

7 Franzmeier N, Rubinski A, Neitzel J, Kim Y, Damm A, Na DL, Kim HJ, Lyoo CH, Cho H, Finsterwalder S *et al*. (2019) Functional connectivity associated with tau levels in ageing, Alzheimer's, and small vessel disease. *Brain* **142**, 1093–1107.

8 Cope TE, Rittman T, Borchert RJ, Jones PS, Vatansever D, Allinson K, Passamonti L, Vazquez Rodriguez P, Bevan-Jones WR, O'Brien JT *et al*. (2018) Tau burden and the functional connectome in Alzheimer's disease and progressive supranuclear palsy. *Brain* **141**, 550–567.

9 La Joie R, Visani AV, Baker SL, Brown JA, Bourakova V, Cha J, Chaudhary K, Edwards L, Iaccarino L, Janabi M *et al*. (2020) Prospective longitudinal atrophy in Alzheimer's disease correlates with the intensity and topography of baseline tau-PET. *Sci Transl Med* **12**, eaau5732.

10 Congdon EE, Kim S, Bonchak J, Songrug T, Matzavinos A & Kuret J (2008) Nucleation-dependent tau filament formation: the importance of dimerisation and an estimation of elementary rate constants. *J Biol Chem* **283**, 13806–13816.

11 Sonawane SK, Uversky VN & Chinnathambi S (2021) Baicalein inhibits heparin-induced Tau aggregation by initialising non-toxic Tau oligomer formation. *Cell Commun Signal* **19**, 16.

12 Habchi J, Arosio P, Perni M, Costa AR, Yagi-Utsumi M, Joshi P, Chia S, Cohen SIA, Müller MBD, Linse S *et al*. (2016) An anticancer drug suppresses the primary nucleation reaction that initiates the production of the toxic Aβ42 aggregates linked with Alzheimer's disease. *Sci Adv* **2**, e1501244.

13 Seidler PM, Boyer DR, Murray KA, Yang TP, Bentzel M, Sawaya MR, Rosenberg G, Cascio D, Williams CK, Newell KL *et al*. (2019) Structure-based inhibitors halt prion-like seeding by Alzheimer's disease–and tauopathy–derived brain tissue samples. *J Biol Chem* **294**, 16451–16464.

14 Bhattacharya K, Rank KB, Evans DB & Sharma SK (2001) Role of cysteine-291 and cysteine-322 in the polymerisation of human tau into Alzheimer-like filaments. *Biochem Biophys Res Comm* **285**, 20–26.

15 Kim D, Lim S, Haque MDM, Ryoo N, Hong HS, Rhim H, Lee D-E, Chang Y-T, Lee J-S, Cheong E *et al*. (2015) Identification of disulfide cross-linked tau dimer responsible for tau propagation. *Sci Rep* **5**, 15231.

16 Soeda Y, Yoshikawa M, Almeida OFX, Sumioka A, Maeda S, Osada H, Kondoh Y, Saito A, Miyasaka T, Kimura T *et al*. (2015) Toxic tau oligomer formation blocked by capping of cysteine residues with 1,2-dihydroxybenzene groups. *Nat Commun* **6**, 10216.

17 Driver JA, Beiser A, Au R, Kreger BE, Splansky GL, Kurth T, Kiel DP, Lu KP, Seshadri S & Wolf PA (2012) Inverse association between cancer and Alzheimer's disease: results from the Framingham Heart Study. *BMJ* **344**, e1442.
18 Musicco M, Adorni F, Di Santo S, Prinelli F, Pettenati C, Caltagirone C, Palmer K & Russo A (2013) Inverse occurrence of cancer and Alzheimer disease: a population-based incidence study. *Neurology* **81**, 322–328.
19 Schmidt SAJ, Ording AG, Horváth-Puhó E, Sørensen HT & Henderson VW (2017) Non-melanoma skin cancer and risk of Alzheimer's disease and all-cause dementia. *PLoS One* **12**, e0171527.
20 Frain L, Swanson D, Cho K, Gagnon D, Lu KP, Betensky RA & Driver J (2017) Association of cancer and Alzheimer's disease risk in a national cohort of veterans. *Alzheimers Dement* **13**, 1364–1370.
21 Ospina-Romero M, Abdiwahab E, Kobayashi L, Filshtein T, Brenowitz WD, Mayeda ER & Glymour MM (2019) Rate of memory change before and after cancer diagnosis. *JAMA Network Open* **2**, e196160.
22 Sun M, Wang Y, Sundquist J, Sundquist K & Ji J (2020) The association between cancer and dementia: a National Cohort Study in Sweden. *Front Oncol* **10**, 73.
23 Lanni C, Masi M, Racchi M & Govoni S (2021) Cancer and Alzheimer's disease inverse relationship: an age-associated diverging derailment of shared pathways. *Mol Psychiatry* **26**, 280–295.
24 Mezencev R & Chernoff YO (2020) Risk of Alzheimer's disease in cancer patients: analysis of mortality data from the US SEER population-based registries. *Cancers (Basel)* **12**, 796.
25 Kwok MK, Lin SL & Schooling CM (2018) Re-thinking Alzheimer's disease therapeutic targets using gene-based tests. *EBioMedicine* **37**, 461–470.
26 Holmes BB, Furman JL, Mahan TE, Yamasaki TR, Mirbaha H, Eades WC, Belaygorod L, Cairns NJ, Holtzman DM & Diamond MI (2014) Proteopathic tau seeding predicts tauopathy in vivo. *Proc Natl Acad Sci USA* **111**, E4376.
27 Johnston PA (2011) Redox cycling compounds generate H2O2 in HTS buffers containing strong reducing reagents—real hits or promiscuous artifacts? *Curr Opin Chem Biol* **15**, 174–182.
28 Hudson SA, Ecroyd H, Kee TW & Carver JA (2009) The thioflavin T fluorescence assay for amyloid fibril detection can be biased by the presence of exogenous compounds. *FEBS J* **276**, 5960–5972.
29 Berger Z, Roder H, Hanna A, Carlson A, Rangachari V, Yue M, Wszolek Z, Ashe K, Knight J, Dickson D *et al.* (2007) Accumulation of pathological tau species and memory loss in a conditional model of tauopathy. *J Neurosci* **27**, 3650.
30 Ganguly P, Do TD, Larini L, LaPointe NE, Sercel AJ, Shade MF, Feinstein SC, Bowers MT & Shea J-E (2015) Tau assembly: the dominant role of PHF6 (VQIVYK) in microtubule binding region repeat R3. *J Phys Chem B* **119**, 4582–4593.
31 Ghag G, Bhatt N, Cantu DV, Guerrero-Munoz MJ, Ellsworth A, Sengupta U & Kayed R (2018) Soluble tau aggregates, not large fibrils, are the toxic species that display seeding and cross-seeding behavior. *Protein Sci* **27**, 1901–1909.
32 Musi N, Valentine JM, Sickora KR, Baeuerle E, Thompson CS, Shen Q & Orr ME (2018) Tau protein aggregation is associated with cellular senescence in the brain. *Aging Cell* **17**, e12840.
33 Miyazaki Y, Mizumoto K, Dey G, Kudo T, Perrino J, Chen L, Meyer T & Wandless TJ (2016) A method to rapidly create protein aggregates in living cells. *Nat Commun* **7**, 11689.
34 Margittai M & Langen R (2004) Template-assisted filament growth by parallel stacking of tau. *Proc Natl Acad Sci USA* **101**, 10278.
35 Natale C, Barzago MM & Diomede L (2020) *Caenorhabditis elegans* models to investigate the mechanisms underlying tau toxicity in tauopathies. *Brain Sci* **10**, 838.
36 Sandhof CA, Hoppe SO, Tittelmeier J & Nussbaum-Krammer C (2020) *C. elegans* models to study the propagation of prions and prion-like proteins. *Biomolecules* **10**, 1188.
37 Rodriguez S, Hug C, Todorov P, Moret N, Boswell SA, Evans K, Zhou G, Johnson NT, Hyman BT, Sorger PK *et al.* (2021) Machine learning identifies candidates for drug repurposing in Alzheimer's disease. *Nat Commun* **12**, 1033.
38 Cummings J, Lee G, Ritter A & Zhong K (2018) Alzheimer's disease drug development pipeline: 2018. *Alzheimers Dement (N Y)* **4**, 195–214.
39 Sun L-M, Chen H-J, Liang J-A & Kao C-H (2016) Long-term use of tamoxifen reduces the risk of dementia: a nationwide population-based cohort study. *QJM* **109**, 103–109.
40 Brunden KR, Yao Y, Potuzak JS, Ferrer NI, Ballatore C, James MJ, Hogan A-ML, Trojanowski JQ, Smith Iii AB & Lee VMY (2011) The characterisation of microtubule-stabilising drugs as possible therapeutic agents for Alzheimer's disease and related tauopathies. *Pharmacol Res* **63**, 341–351.
41 Huang L, Lin J, Xiang S, Zhao K, Yu J, Zheng J, Xu D, Mak S, Hu S, Nirasha S *et al.* (2016) Sunitinib, a clinically used anticancer drug, is a potent AChE inhibitor and attenuates cognitive impairments in mice. *ACS Chem Neurosci* **7**, 1047–1056.
42 Cramer PE, Cirrito JR, Wesson DW, Daniel Lee CY, Karlo JC, Zinn AE, Casali BT, Restivo JL, Goebel WD, James MJ *et al.* (2012) ApoE-directed therapeutics

rapidly clear β-amyloid and reverse deficits in AD mouse models. *Science* **335**, 1503–1506.
43 O'Hare E, Jeggo R, Kim E-M, Barbour B, Walczak J-S, Palmer P, Lyons T, Page D, Hanna D, Meara JR *et al.* (2016) Lack of support for bexarotene as a treatment for Alzheimer's disease. *Neuropharmacology* **100**, 124–130.
44 Hayes CD, Dey D, Palavicini JP, Wang H, Patkar KA, Minond D, Nefzi A & Lakshmana MK (2013) Striking reduction of amyloid plaque burden in an Alzheimer's mouse model after chronic administration of carmustine. *BMC Med* **11**, 81.
45 Chu J, Lauretti E, Craige CP & Praticò D (2014) Pharmacological modulation of GSAP reduces amyloid-β levels and tau phosphorylation in a mouse model of Alzheimer's disease with plaques and tangles. *J Alzheimers Dis* **41**, 729–737.
46 Hernandez I, Luna G, Rauch JN, Reis SA, Giroux M, Karch CM, Boctor D, Sibih YE, Storm NJ, Diaz A *et al.* (2019) A farnesyltransferase inhibitor activates lysosomes and reduces tau pathology in mice with tauopathy. *Sci Transl Med* **11**, eaat3005.
47 Bulic B, Pickhardt M, Schmidt B, Mandelkow E-M, Waldmann H & Mandelkow E (2009) Development of tau aggregation inhibitors for Alzheimer's disease. *Angew Chem Int Ed* **48**, 1740–1752.
48 Lasagna-Reeves CA, Castillo-Carranza DL, Guerrero-Muñoz MJ, Jackson GR & Kayed R (2010) Preparation and characterisation of neurotoxic tau oligomers. *Biochemistry* **49**, 10039–10041.
49 Kaniyappan S, Chandupatla RR, Mandelkow E-M & Mandelkow E (2017) Extracellular low-n oligomers of tau cause selective synaptotoxicity without affecting cell viability. *Alzheimers Dement* **13**, 1270–1291.
50 Flach K, Hilbrich I, Schiffmann A, Gärtner U, Krüger M, Leonhardt M, Waschipky H, Wick L, Arendt T & Holzer M (2012) Tau oligomers impair artificial membrane integrity and cellular viability *. *J Biol Chem* **287**, 43223–43233.
51 Xu M, Pirtskhalava T, Farr JN, Weigand BM, Palmer AK, Weivoda MM, Inman CL, Ogrodnik MB, Hachfeld CM, Fraser DG *et al.* (2018) Senolytics improve physical function and increase lifespan in old age. *Nat Med* **24**, 1246–1256.
52 Yamada K, Cirrito JR, Stewart FR, Jiang H, Finn MB, Holmes BB, Binder LI, Mandelkow E-M, Diamond MI, Lee VM-Y *et al.* (2011) In Vivo microdialysis reveals age-dependent decrease of brain interstitial fluid tau levels in P301S human tau transgenic mice. *J Neurosci* **31**, 13110.
53 Annadurai N, De Sanctis JB, Hajdúch M & Das V (2021) Tau secretion and propagation: perspectives for potential preventive interventions in Alzheimer's disease and other tauopathies. *Exp Neurol* **343**, 113756.
54 Nečas D & Klapetek P (2012) Gwyddion: an open-source software for SPM data analysis. *Cent Eur J Phys* **10**, 181–188.
55 Fitzpatrick AWP, Falcon B, He S, Murzin AG, Murshudov G, Garringer HJ, Crowther RA, Ghetti B, Goedert M & Scheres SHW (2017) Cryo-EM structures of tau filaments from Alzheimer's disease. *Nature* **547**, 185–190.
56 Šali A & Blundell TL (1993) Comparative protein modelling by satisfaction of spatial restraints. *J Mol Biol* **234**, 779–815.
57 Frisch MJ, Trucks GW, Schlegel HB, Scuseria GE, Robb MA, Cheeseman JR, Scalmani G, Barone V, Petersson GA, Nakatsuji H *et al.* (2016) F Gaussian 09, Revision A.02. Gaussian, Inc., Wallingford, CT.
58 Case DA, Darden TA, Cheatham TE III, Simmerling CL, Wang J, Duke RE, Luo R, Walker RC, Zhang W, Merz KM *et al.* (2010) AMBER 11. University of California, San Francisco, CA.
59 Bayly CI, Cieplak P, Cornell W & Kollman PA (1993) A well-behaved electrostatic potential based method using charge restraints for deriving atomic charges: the RESP model. *J Phys Chem* **97**, 10269–10280.
60 Trott O & Olson AJ (2010) AutoDock Vina: improving the speed and accuracy of docking with a new scoring function, efficient optimisation, and multithreading. *J Comput Chem* **31**, 455–461.
61 Maier JA, Martinez C, Kasavajhala K, Wickstrom L, Hauser KE & Simmerling C (2015) ff14SB: improving the accuracy of protein side chain and backbone parameters from ff99SB. *J Chem Theory Comput* **11**, 3696–3713.
62 Ryckaert J-P, Ciccotti G & Berendsen HJC (1977) Numerical integration of the cartesian equations of motion of a system with constraints: molecular dynamics of n-alkanes. *J Comput Phys* **23**, 327–341.
63 Allen MP & Tildesley DJ (1991) Computer Simulation of Liquids. Oxford University Press, New York, NY.
64 Berendsen HJC, Postma JPM, van Gunsteren WF, DiNola A & Haak JR (1984) Molecular dynamics with coupling to an external bath. *J Chem Phys* **81**, 3684–3690.
65 Darden T, York D & Pedersen L (1993) Particle mesh Ewald: an N·log(N) method for Ewald sums in large systems. *J Chem Phys* **98**, 10089–10092.
66 Ester M, Kriegel H-P, Sander J & Xiaowei X (1996) A density-based algorithm for discovering clusters in large spatial databases with noise. In In Proceedings of the Second International Conference on Knowledge Discovery and Data Mining (Simoudis E, Han J & Fayyad U, eds), pp. 226–231. AAAI Press.
67 Seidler PM, Boyer DR, Rodriguez JA, Sawaya MR, Cascio D, Murray K, Gonen T & Eisenberg DS (2018) Structure-based inhibitors of tau aggregation. *Nat Chem* **10**, 170–176.

68 Diomede L, Rognoni P, Lavatelli F, Romeo M, del Favero E, Cantù L, Ghibaudi E, di Fonzo A, Corbelli A, Fiordaliso F *et al*. (2014) A *Caenorhabditis elegans*–based assay recognises immunoglobulin light chains causing heart amyloidosis. *Blood* **123**, 3543.

Supporting information

Additional supporting information may be found online in the Supporting Information section at the end of the article.

Fig. S1. Dose-dependent effect of drugs and DMSO effect on aggregation.
Fig. S2. Data on mutant R3 peptide aggregation.
Fig. S3. Raw data of seeding from Fig. 6 and drug-only effect on cell viability.
Fig. S4. Raw data of cell number from Fig. 7.
Fig. S5. Data showing pharyngeal impairment is transient.
Appendix S1. Methods.